Resonance parameters of ^{60}Ni+n from measurements of transmission and capture yields from 1 to 450 keV

C. M. Perey, J. A. Harvey, R. L. Macklin, and F. G. Perey
Oak Ridge National Laboratory, Oak Ridge, Tennessee 37830

R. R. Winters
Denison University, Granville, Ohio 43203

(Received 7 February 1983)

High-resolution transmission and capture measurements of ^{60}Ni-enriched targets have been made from a few eV to 1800 keV in transmission and from 2.5 keV to 5 MeV in capture. The transmission data from 1 to 452 keV were analyzed with a multilevel R-matrix code which uses Bayes' theorem for the fitting process. This code provides the energies and neutron widths of the resonances inside the 1- to 452-keV region as well as a possible parametrization for outside resonances to describe the smooth cross section in this region. The capture data were analyzed from 2.5 to 452 keV with a least-squares fitting code using the Breit-Wigner formula. Average parameters for the 30 observed s-wave resonances were deduced. The average level spacing, D_0, was found to be equal to 15.2±1.5 keV; the strength function, S_0, equal to $(2.2\pm0.6)\times10^{-4}$; and the average radiation width, $\overline{\Gamma}_\gamma$, equal to 1.30±0.07 eV. The staircase plot of the reduced level widths and the plot of the Lorentz-weighted strength function averaged over various energy intervals show possible evidence for doorway states. The level densities calculated with the Fermi-gas model for $l=0$ and for $l>0$ resonances were compared with the cumulative number of observed resonances, but the analysis is not conclusive. The correlation coefficient ρ between Γ_n^0 and Γ_γ is equal to 0.53±0.18. The average capture cross section as a function of the neutron incident energy is compared to the tail of the giant electric dipole resonance prediction.

[NUCLEAR REACTIONS ^{60}Ni(n,n), E_n=1–452 keV; ^{60}Ni(n,γ), E_n=2.5–452 keV; measured $\sigma_{n,\mathrm{tot}}(E_n)$, $\sigma_{n,\gamma}(E_n)$; deduced ^{61}Ni resonance parameters E_0, $g\Gamma_n$, Γ_γ, l, J, and average properties D_0, S_0, $\overline{\Gamma}_\gamma$; calculated level density for $l=0$ and $l>0$ resonances and correlation $\rho(\Gamma_n^0,\Gamma_\gamma)$.]

I. INTRODUCTION

The cross sections of structural materials in the iron region are important in reactor applications because of the stainless steels that are used. In the Evaluated Nuclear Data File (ENDF), the current evaluation of the nickel resonance parameters[1] (ENDF/B-V) is based on measurements taken prior to 1971 and is identical to ENDF/B-IV and ENDF/B-III versions.

High-resolution total and capture measurements on the nickel isotopes were performed at the Oak Ridge Electron Linear Accelerator (ORELA) in the resonance region. In this paper we present the analysis of the ^{60}Ni data and compare the results with previously published resonance parameters.

In this work we emphasize the features of the analysis specific to a recently available multilevel R-matrix code, to be described later, which uses Bayes' theorem for the fitting process of the transmission data. Even though the transmission and capture data were analyzed with two different codes, the final resonance parameters were obtained through an iterative process between the two analyses in order to ensure consistency and to optimize the use of the information available in both data sets. A fully documented Oak Ridge National Laboratory (ORNL) report[2] has been published and should be consulted for more details.

The average resonance parameters of the s-wave resonances have been studied, and their behavior shows possible evidence of doorway states.

II. TRANSMISSION MEASUREMENTS AND DATA PROCESSING

The transmission measurements were made by the time-of-flight technique using neutron pulses from

the ORELA water-moderated tantalum target and a 78.203-m flight path. Measurements were made on two samples of ^{60}Ni enriched to 99.79% with thicknesses of 0.007 36 and 0.0744 atoms/barn. Two different neutron detectors and techniques were used to cover the energy region investigated. (See Ref. 2 for more details.)

For the energy region from 200 eV to 240 keV, transmission data were acquired using a 1.3-cm-thick, 11-cm-diameter ^{6}Li glass scintillation detector. The electron beam burst was 40 ns wide, producing a beam power on the target of 40 kW at 800 Hz. The equivalent spread in flight path due to the moderator was 20 mm full width at half maximum (FWHM). Two filters were inserted in the beam at 5 m: a 1-g/cm^2 ^{10}B filter ($1/e$ transmission at ~ 1 keV) to eliminate low-energy neutrons from preceding bursts, and a 0.6-cm-thick lead filter to reduce the gamma flash.

By use of a 2-cm-thick, 7.5-cm-diameter NE-110 proton recoil scintillation detector,[3] transmission data were obtained from 4 to 1770 keV. The electron beam burst was 10-ns wide, producing a beam power of 16 kW at 1000 Hz. The energy resolution $\Delta E/E$ obtained with the NE-110 scintillator was 0.1% below 100 keV and 0.35 $[E\ (\mathrm{MeV})]^{1/2}$% at higher energies. (See Table I for sample values of neutron energy resolution.) Two filters were inserted in the neutron beam at 5 m: the 1-g/cm^2 ^{10}B filter and a 0.6-cm-thick ^{238}U filter. The detectors were gated off during the gamma flash and the succeeding ~ 5 μs to reduce interference due to afterpulsing.

During the measurements three sources of backgrounds were monitored: (1) a background arising from 2.2-MeV gamma rays produced by neutron capture in the water moderator of the target; (2) a time and beam independent room background; and (3) a background produced by neutrons scattered by the detector which, with the NE-110 detector, arises mainly from a 478-keV gamma ray from the ^{10}B$(n,\alpha\gamma)$ reaction produced from the absorption of neutrons by the boron in the Pyrex face of the photomultiplier. To aid in the determination of these backgrounds and to optimize the signal to background ratio for the NE-110 detector, four separate pulse-height spectra were recorded. The contribution of all of these backgrounds was $< 1\%$ over the energy region where the data were analyzed. Additional details on corrections for these backgrounds are given in Refs. 4 and 5.

All time-of-flight data were acquired using an EG&G time digitizer and stored in one of the ORELA Data Acquisition Computers.[6] The data were first corrected for the deadtime (1104 ns) of the time digitizer and then corrected for the backgrounds discussed above. The transmission and total cross section are computed from the background corrected sample-in—sample-out ratio normalized to the same monitor counts. Results, up to 450 keV, are shown in Figs. 1 to 7.

TABLE I. Sample values of neutron energy resolution, ΔE (full width at half maximum), in the transmission and capture experiments.

E_n (keV)	Transmission expt. Detector	ΔE (eV)	Capture expt. ΔE (eV)
10	^{6}Li	15	10
30	^{6}Li	75	46
50	^{6}Li	80	
	NE-110	50	
100	NE-110	130	173
200	NE-110	333	390
400	NE-110	927	949

III. TRANSMISSION DATA ANALYSIS

The transmission data were first analyzed with the multilevel R-matrix least-squares fitting code MULTI.[7] When this analysis and the analysis of the capture data described in Sec. V were completed, the code SAMMY,[8] a modified version of MULTI, became available and was used to obtain the final fits to the transmission data and the corresponding neutron widths reported here.

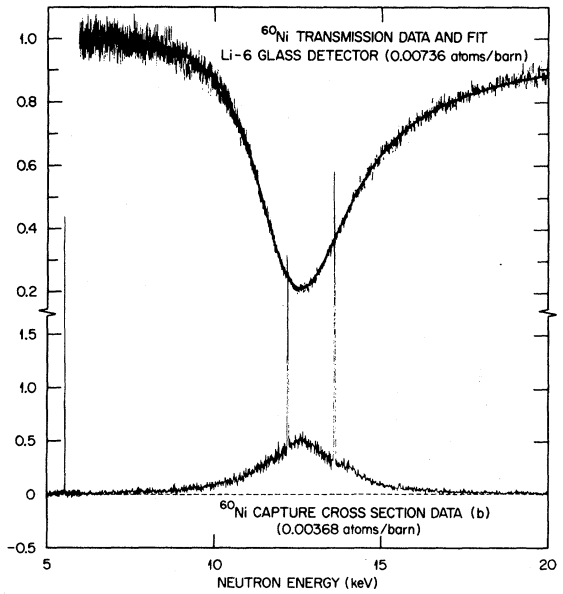

FIG. 1. ^{60}Ni transmission data and fit shown with the capture data from 5 to 20 keV.

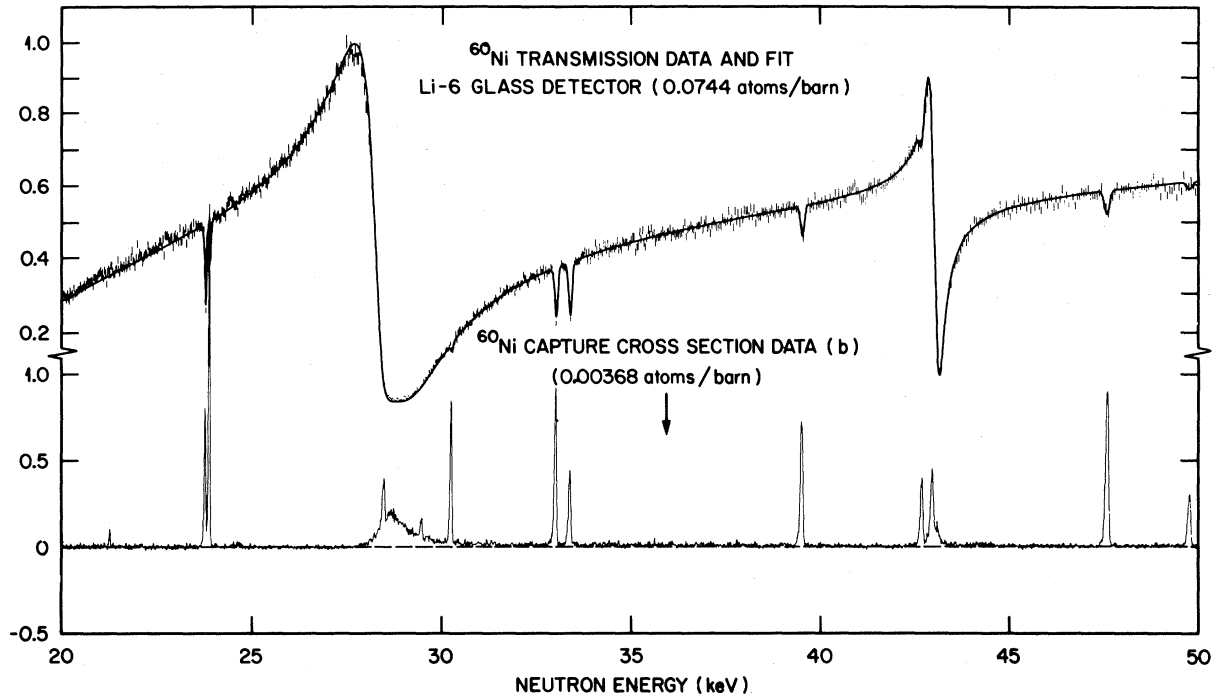

FIG. 2. ^{60}Ni transmission data and fit shown with the capture data from 20 to 50 keV.

In both codes Doppler- and resolution-broadening are calculated. The cross section is expressed as

$$\sigma_T=\Sigma\sigma_{nT}=2\pi k^{-2}\sum_J g(J)\mathrm{Re}(1-U_{nn}^J)\,, \qquad (3.1)$$

and

$$U_{nn}^J=e^{-2i\phi_l}\frac{1-R_l^J(S_l-B_l^J-iP_l)}{1-R_l^J(S_l-B_l^J+iP_l)}\,, \qquad (3.2)$$

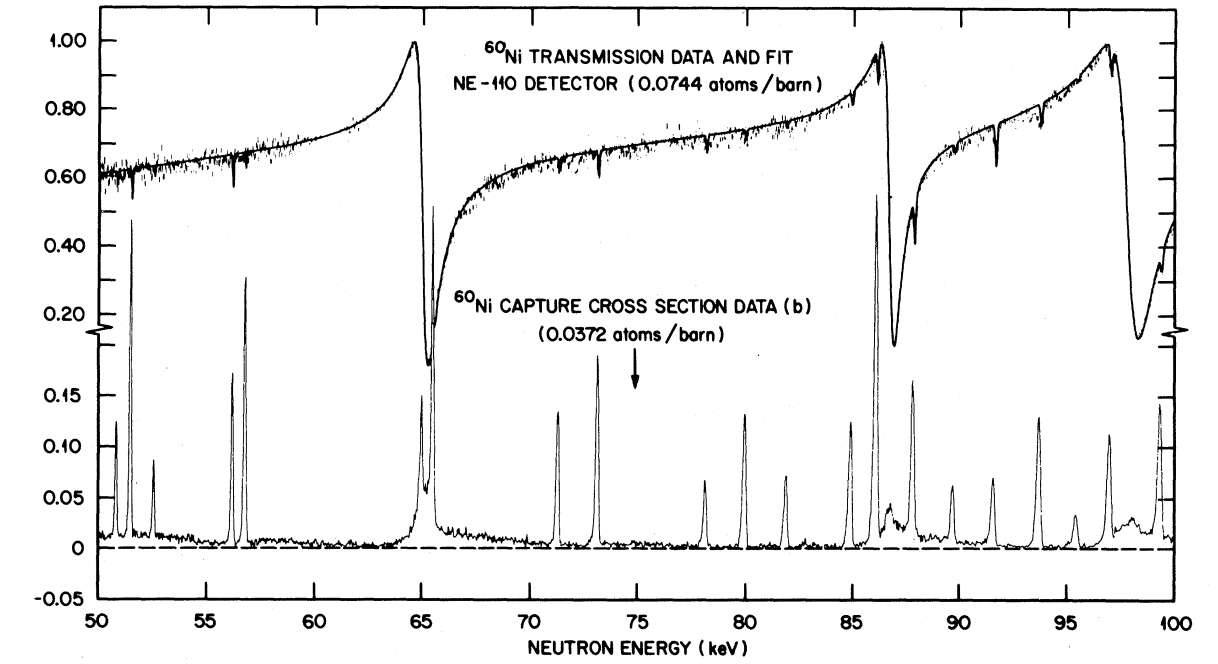

FIG. 3. ^{60}Ni transmission data and fit shown with the capture data from 50 to 100 keV.

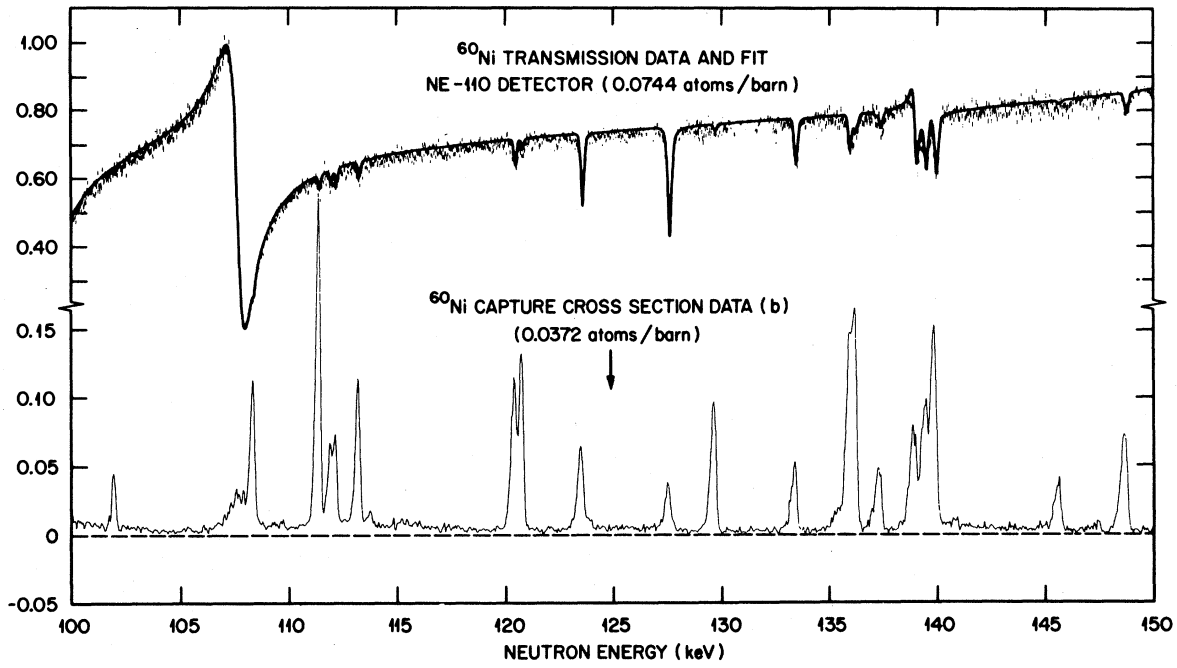

FIG. 4. ^{60}Ni transmission data and fit shown with the capture data from 100 to 150 keV.

$$R_l^J = \sum_\lambda \frac{\gamma_{l\lambda}^2}{E_\lambda - E - i\Gamma_{\gamma\lambda}/2} \,. \tag{3.3}$$

Here R_l^J is the reduced R matrix; k is the neutron wave number, assuming that the only open channels are elastic neutron scattering and photon emission; and $\gamma_{l\lambda}$ and $\Gamma_{\gamma\lambda}$ are the neutron reduced width amplitude and the radiation width, respectively, for the λth resonance. The ϕ_l, S_l, B_l, and P_l represent the usual hard sphere phase shifts, shift factors, boundary conditions, and neutron penetrability, respectively. The codes used in this analysis give the neutron width $\Gamma_{n\lambda}$ for each resonance which is related to the neutron reduced width amplitude $\gamma_{l\lambda}$ by the

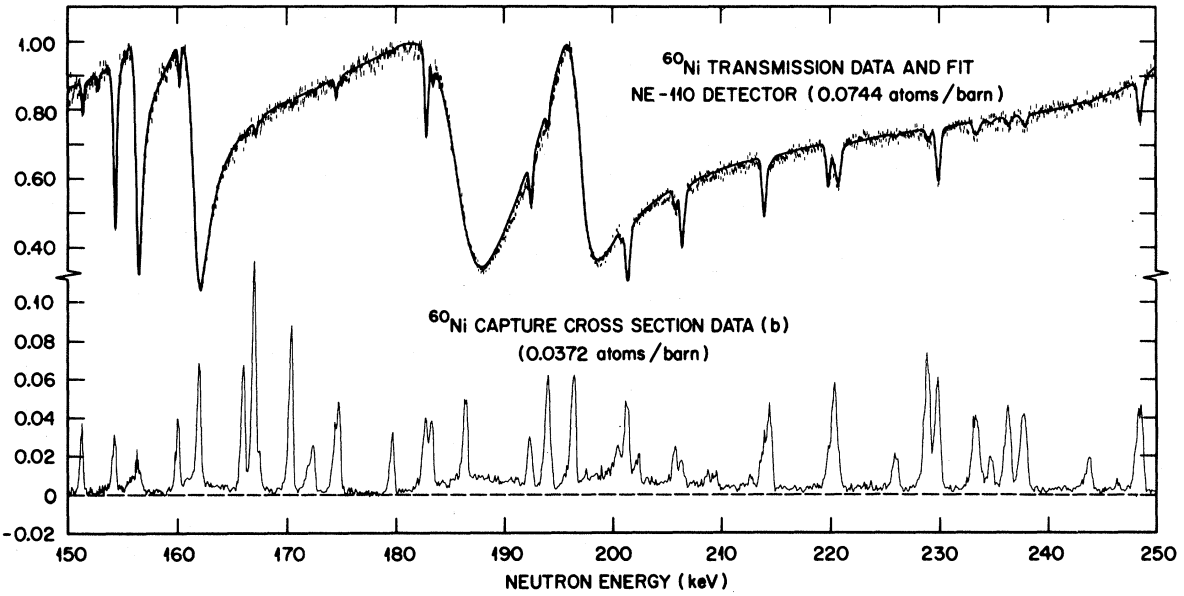

FIG. 5. ^{60}Ni transmission data and fit shown with the capture data from 150 to 250 keV.

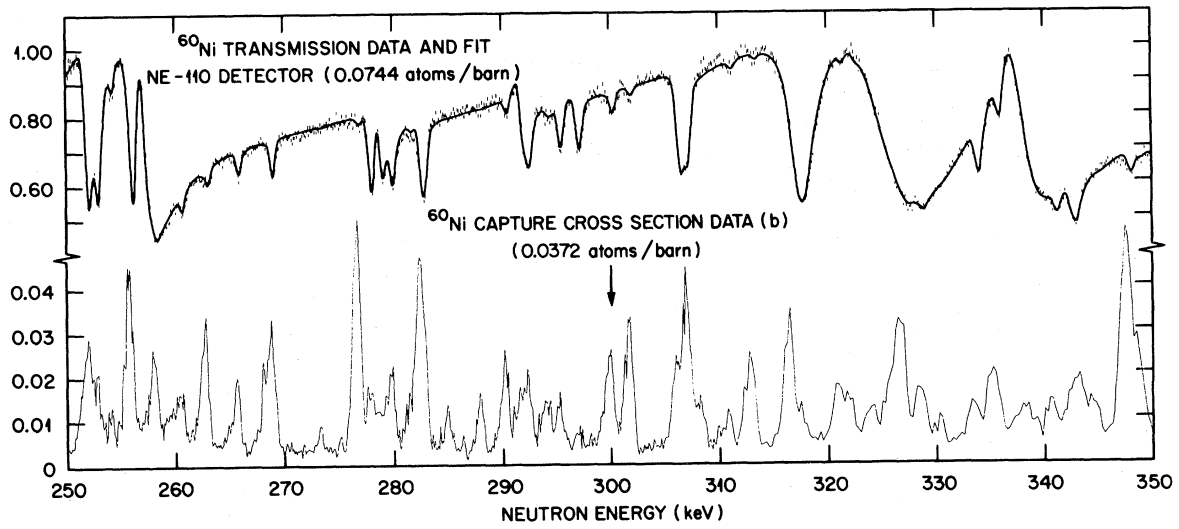

FIG. 6. ^{60}Ni transmission data and fit shown with the capture data from 250 to 350 keV.

relation

$$\Gamma_{n\lambda}=2\gamma_{l\lambda}{}^2P_l \ .$$

The first excited state at 1332.5 keV is well above the energy range of our analysis, so inelastic scattering channels could be ignored.

In this work, S_l and B_l^J are set equal. This is often done although S_l is energy dependent whereas B_l^J is a constant and, strictly speaking, they can only be equal at one energy. The channel radius was set equal to 6.0 fm from a preliminary analysis up to 150 keV where the radius was adjusted.

The code SAMMY was developed to cope with a practical problem encountered in the analysis of the data with the code MULTI. This problem occurred because MULTI is a nonlinear least-squares code and because all the transmission data could not be fitted simultaneously. When analyzing a particular energy region of the data, if one allows all of the resonance parameters inside and outside the region to be adjusted to obtain a fit to this energy region, one obtains a good fit for this energy region, but the fit to the previously analyzed energy regions is destroyed. There is no way to communicate to MULTI how to vary resonance parameters to improve the fit in a particular energy region being analyzed in such a way that the fits to the data previously analyzed will not be destroyed. The code SAMMY solves this problem.

SAMMY is a constrained least-squares code which,

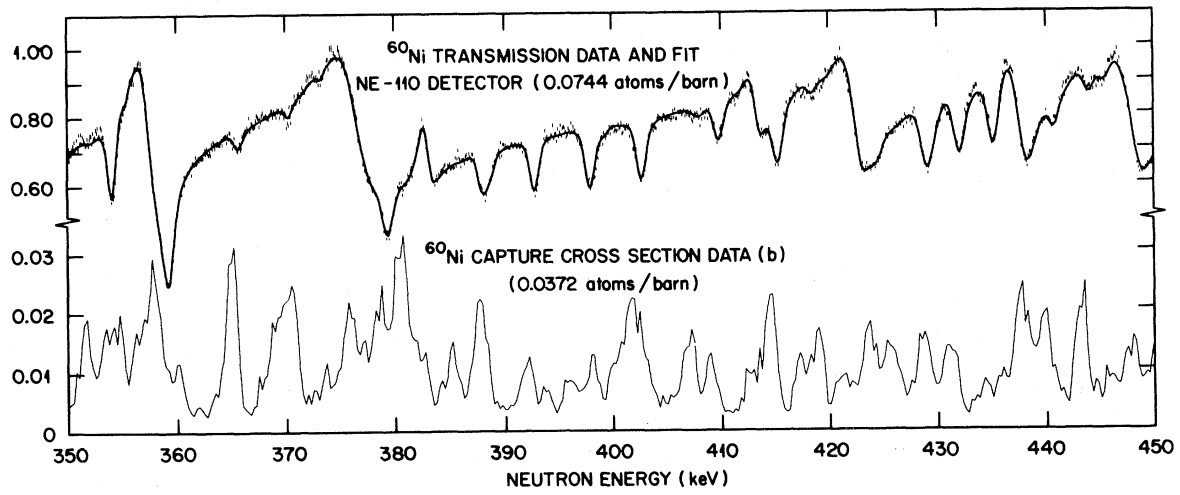

FIG. 7. ^{60}Ni transmission data and fit shown with the capture data from 350 to 450 keV.

in principle, produces an output of a sequential analysis of all the energy regions of the data the same as if all the energy regions had been analyzed simultaneously. SAMMY achieves this result by solving Bayes' equation which makes use of the covariance matrix of the parameters being varied (obtained as the output of the previously analyzed energy regions) to vary the parameters of the resonances to fit a new energy region. The major difference between the two codes from an operational point of view is that in SAMMY one must input not only a resonance parameter file but also a covariance matrix for these resonance parameters. It is this covariance matrix of the input parameters that allows SAMMY to vary the resonance parameters to fit a new energy region without destroying the fit to previously analyzed energy regions.

The transmission data analyzed between 1 and 50 keV were those obtained with the ^{6}Li detector. Data obtained with the thick sample of ^{60}Ni (0.0744 atoms/barn) were used from 1 to 6 keV and from 20 to 50 keV. From 6 to 20 keV, the data obtained with the thin sample (0.007 36 atoms/barn) were analyzed. Above 50 keV, the data obtained with the NE-110 detector and the thick sample were analyzed.

All resonances showing the characteristic potential interference of s waves were assigned as s waves. Up to 230 keV, all other resonances could be fitted assuming they were $p_{1/2}$ resonances but they are essentially $l>0$ resonances. Above 230 keV, all non—s-wave resonances were first fitted assuming they were $p_{1/2}$ resonances. If a satisfactory fit could not be obtained, the assignment of $d_{3/2}$ was tried and adopted if the fit was improved. Above 230 keV, because of increasing potential scattering, the transmission data show some sensitivity to p-wave assignment through the interference term. Only in some instances was this sensitivity large enough that the resonances assigned as $d_{3/2}$ are very likely neither $p_{1/2}$ nor $p_{3/2}$. However, the situation is more complex in the case of multiplets because the data may only have been sensitive to level-level interference rather than to the potential interference. Therefore, in case of multiplets the assignment of levels as $p_{1/2}$ or $d_{3/2}$ may be very misleading because it may be that the data could have been fitted just as well with a $p_{3/2}$ assignment for the level assigned $d_{3/2}$, or other combination of J^π values. As expected, the number of $d_{3/2}$ resonances found necessary for a good fit increases with energy. Around 400 keV, as many d as p resonances were assigned. Higher resolution transmission data and measurements of the differential elastic scattering cross sections[9,10] would be necessary to assign spin and parity to $l>0$ resonances.

The set of parameters obtained in a preliminary analysis with the code MULTI reproduced well the transmission data from 1 to 550 keV. The results of this preliminary analysis were combined with the results of the capture analysis reported in Sec. V to obtain the input parameter file of the code SAMMY. This input file contained 273 resonances. A total of 203 parameters was allowed to be adjusted by the code during the analysis. Four of the 273 resonances were outside the 1 to 550 keV energy region and 89 were seen in the capture data only. The parameters of these 89 resonances were not adjusted by the code. They were included in the parameter file in order to check that the values assigned to Γ_n and Γ_γ were also consistent with the transmission data. Some were not and had to be readjusted by trial and error. For some of these resonances, we were able to estimate the upper limit of Γ_n. For example, we can see in Fig. 3 that the parameters given in Table II for the resonances at 50.927, 56.880, 71.370, 78.217, and 84.990 keV give the maximum acceptable dip in the theoretical transmission to stay compatible with the data. It should be understood that the set of values for Γ_n and Γ_γ assigned to the resonances seen only in the capture data is not unique since only the capture area is well defined. When possible, a value of 0.5 eV was assigned to the radiation width of these resonances. Above 450 keV, where no analysis of the capture data was performed, an arbitrary value of 2 eV was assigned to the radiation widths of all resonances. The input covariance matrix of the parameters had only diagonal elements.

Running the code SAMMY with these input parameter and covariance files (or similar ones obtained at the end of each run) and with data files of about 300 points ($\sim$50 keV range) took an average of 1 h of computing time on the ORELA PDP-10(KA). As new information was fed to the code through the data, the resonance parameters became better known and more correlated. The covariance matrix of the parameters increased in size (up to 13 print-out pages) as more nondiagonal elements were determined. Because of its size, the complete covariance matrix of the parameters cannot be given here. The main results are discussed in Sec. VII.

Above 300 keV the smooth behavior of the transmission between the sharp resonances is strongly influenced by the tail of the large fictitious resonance originally set at 607 keV. As the analysis progressed from the lowest energy regions to the highest, the energy of this resonance was readjusted by the code towards lower energies. At the completion of the 400- to 450-keV region analysis, the parameters of this resonance were $E=450\pm2$ keV and $\Gamma_n=79\pm1$ keV. At that point, difficulties in

TABLE II. Resonance parameters for ^{60}Ni+n from 1 to 452 keV. (Columns are fully identified in Sec. VII A.)

E_0[a] (keV) $s_{1/2}$	$p_{1/2}$	$d_{3/2}$	$g\Gamma_n\Gamma_\gamma/\Gamma$ (eV)	$g\Gamma_n$ (eV)	Γ_γ (eV)	C (10^{-3})	$\Gamma_{\gamma(\mathrm{corr})}$ (eV)
−50				14 800(70)			
−0.15(11)				0.86(25)	1.5		
	2.253(1)[e]			0.053(1)	1.20(8)		
	5.532(1)		0.043(3)	0.045(3)	1.0(6)		
	12.220(1)[b]		0.201(4)	0.34	0.50[d]		
12.487(1)			4.3(2)	2358(3)	4.3(2)	0.72	2.6(9)
	13.624(1)[b]		0.353(6)	1.20	0.50[d]		
	21.274(2)[b]		0.022(2)	0.023	0.50[d]		
	23.788(1)		0.24(1)	4.5(2)	0.25(1)		
	23.898(1)		0.54(1)	1.17(4)	1.0(1)		
	[28.458(2)[b]		0.04(2)[c]	0.05	0.50[d]		
	[28.497(2)[b]		0.11(2)	0.14	0.50[d]		
28.709(1)			1.6(1)	698.(1)	1.6(1)	1.3	0.7(5)
	29.480(2)[b]		0.061(5)	0.069	0.50[d]		
	30.262(1)		0.39(1)	1.0(3)[c]	0.63(2)		
	33.017(2)		0.56(1)	7.7(3)	0.60(1)		
	33.393(2)		0.29(1)	10.0(3)	0.30(1)		
	39.534(1)		0.57(1)	2.3(1)	0.76(2)		
	42.705(1)		0 35(5)	1.6(2)[c]	0.45(3)		
	42.985(2)[b]		0.37(4)	2	0.50[d]		
43.105(1)			0.26(2)	104.4(6)	0.26(2)	0.58	0.20(4)
	[47.567(5)[b]		0.08(1)[c]	0.1	0.50[d]		
	[47.621(3)		0.63(6)[c]	1.1(2)[c]	1.5		
	[47.637(5)		0.31(3)[c]	0.64(10)[c]	0.60		
	49.801(1)[b]		0.36(1)	≤0.6	0.90		
	50.927(2)[b]		0.185(7)	≤0.29	0.50[d]		
	51.594(1)		0.50(1)	0.85(5)[c]	1.21(5)		
	52.658(3)[b]		0.110(7)	≤0.14	0.50[d]		
	56.290(1)		0.32(1)	0.69(5)[c]	0.60(2)		
	56.880(1)[b]		0.52(1)	≤0.62	3.2		
	[64.918(10)[b]		0.05(2)[c]	0.05	0.50[d]		
	[65.053(6)[b]		0.24(7)	0.47	0.50[d]		
65.228(1)			1.10(5)	443.0(8)	1.10(5)	0.35	0.94(9)
	65.573(2)[b]		1.09(8)	≤2.4	2.0		
	71.370(2)[b]		0.41(1)	≤0.75	0.93		
	73.206(1)		0.61(1)	2.0(1)	0.87(3)		
	78.217(2)[b]		0.24(1)	≤0.80	0.34		
	80.048(2)[b]		0.52(1)	≤0.90	1.2		
	81.974(3)[b]		0.27(1)	0.45	0.66		
	84.990(10)[b]		0.52(2)	≤1.0	1.1		
	86.170(2)		1.49(10)	3.0(2)[c]	2.9(4)		
86.837(1)			0.80(5)	398(1)	0.80(5)	0.46	0.62(10)
	87.891(2)		0.9(2)	11.6(3)	1.0(2)		
	89.751(5)[b]		0.28(1)	≤0.50	0.64		
	91.662(5)		0.40(1)	6.5(2)	0.43(1)		
	93.773(5)		0.73(2)	2.7(5)[c]	1.01(3)		
	95.504(5)[b]		0.18(1)	0.28	0.50[d]		
	97.059(5)		0.62(9)	2.9(1)	0.8(2)		
98.085(1)			1.5(1)	1002(2)	1.5(1)	0.60	0.9(3)
	99.405(5)		1.1(1)	7.4(3)	1.3(1)		
	102.064(7)[b]		0.25(2)	≤0.5	0.50[d]		
107.85(<1)			1.15(6)	649(1)	1.15(6)	0.55	0.8(2)
	108.453(5)[b]		0.98(10)	≤0.5	1.2		
	111.47(1)		2.00(5)	4.0(5)[c]	4.0(1)		

TABLE II. (*Continued.*)

E_0[a] (keV) $s_{1/2}$	$p_{1/2}$	$d_{3/2}$	$g\Gamma_n\Gamma_\gamma/\Gamma$ (eV)	$g\Gamma_n$ (eV)	Γ_γ (eV)	C (10^{-3})	$\Gamma_{\gamma(\mathrm{corr})}$ (eV)
	112.00(1)		0.39(3)	2.5(5)[c]	0.46(4)		
	112.24(1)		0.56(3)	3.5(5)[c]	0.66(5)		
	113.320(5)		0.90(3)	3.0(5)[c]	1.27(7)		
	113.87(2)[b]		0.08(2)[c]	0.10	0.50[d]		
	120.52(1)		0.98(3)	7.5(3)	1.13(4)		
	120.85(1)		1.25(3)	2.6(2)	2.39(8)		
	123.618(5)		0.78(4)	31.5(5)	0.80(4)		
	127.66(1)		0.48(2)	67.4(5)	0.49(2)	0.48	0.46(3)
	129.77(1)[b]		1.02(3)	$\leq$2.5	1.7		
	133.52(1)		0.63(3)	20.9(4)	0.65(3)		
	135.46(2)[b]		0.12(2)	0.16	0.50[d]		
	136.03(1)		1.34(5)	15.5(4)	1.45(8)		
	136.29(1)		1.93(8)	6.7(3)	2.7(1)		
	137.21(2)[b]		0.10(1)	$\leq$1.0	0.11		
	137.47(1)		0.58(3)	5.6(3)	0.65(5)		
139.03(<1)			1.14(6)	30.7(5)	1.18(6)		
	139.56(2)		1.22(6)	26.2(5)	1.28(7)		
	140.01(1)		2.23(6)	31.6(5)	2.4(1)		
	145.72(1)[b]		0.50(2)	1.0	1.0[d]		
	147.53(2)[b]		0.09(2)[c]	0.1	0.50[d]		
	148.80(1)		1.13(4)	8.5(3)	1.30(5)		
	151.40(1)		0.49(2)	14.6(4)	0.51(2)		
	152.78(5)[e]		$\leq$0.05	5.9(5)[c]			
	154.35(1)		0.62(3)	162.6(8)	0.62(3)	0.32	0.57(4)
156.36(<1)			0.5(1)[c]	472(1)	0.5(1)	0.31	0.35(13)
	156.48(2)[b]		0.2(1)[c]	0.3	0.50[d]		
	160.22(1)		0.67(15)	20.4(5)	0.70(16)		
161.74(<1)			0.9(1)[c]	1325(2)	0.9(1)	0.33	0.46(25)
	162.15(2)[b]		1.4(2)	10	1.7[d]		
	166.22(1)[b]		1.34(4)	$\leq$3	2.5		
	167.21(1)		2.60(5)	7.4(8)[c]	4.0(1)		
	167.69(2)[b]		0.35(2)	1.2	0.50[d]		
	170.57(1)		1.82(5)	4(1)[c]	3.3(2)		
	172.10(2)[b]		0.22(2)	0.39	0.50[d]		
	172.63(2)[b]		0.53(3)	1.1	1.0[d]		
	174.59(2)		0.46(4)	12.3(5)	0.48(4)		
	174.99(2)		0.93(4)	2.0(5)[c]	1.7(1)		
	179.90(2)[b]		0.62(3)	1.6	1.0[d]		
	182.92(2)		0.91(8)	77.2(8)	0.92(8)		
	183.52(2)		0.83(6)	12.7(5)	0.89(7)		
186.51(<1)			4.0(5)[c]	5237(6)	4.0(5)	0.21	2.9(8)
	186.67(1)[b]		1.1(1)	$\leq$2	2.4		
	191.07(10)[b]		0.13(6)[c]	0.25	0.25[d]		
	192.59(2)		0.78(6)	62.2(8)	0.79(6)		
	194.19(1)		1.65(7)	19.9(6)	1.8(1)		
	194.54(3)[b]		0.25(10)[c]	0.5	0.50[d]		
	196.58(1)[b]		1.7(2)	$\leq$5	2.5		
197.64(<1)			1.8(2)	3025(5)	1.8(2)	0.205	1.2(4)
	199.87(6)[b]		0.2(1)	0.4	0.50[d]		
200.59(3)			0.6(2)	9.8(3)	0.6(2)		
	201.02(3)		0.10(5)[c]	7.4(5)	0.10(5)		
	201.50(3)		2.0(3)	156(2)	2.1(3)		
	202.54(3)[b]		0.43(14)	3	0.50[d]		
	205.93(3)		0.64(5)	36(1)	0.65(6)		
	206.51(3)		0.56(5)	141(1)	0.56(5)	0.20	0.53(5)
	208.93(5)[b]		0.20(3)	0.33	0.50[d]		
	209.68(5)[b]		0.18(3)	0.29	0.50[d]		

TABLE II. (*Continued*.)

E_0[a] (keV)							
$s_{1/2}$	$p_{1/2}$	$d_{3/2}$	$g\Gamma_n\Gamma_\gamma/\Gamma$ (eV)	$g\Gamma_n$ (eV)	Γ_γ (eV)	C (10^{-3})	$\Gamma_{\gamma(\mathrm{corr})}$ (eV)
	212.89(5)[b]		0.21(3)	0.35	0.50[d]		
	214.10(3)		0.76(5)	120(1)	0.77(5)	0.19	0.75(5)
	214.69(2)		1.36(6)	4(1)[c]	2.0(1)		
	220.03(3)		0.28(5)	76(1)	0.28(5)	0.19	0.26(5)
	220.60(2)		1.85(9)	33(1)	1.96(10)		
	220.93(2)		0.67(7)	65(1)	0.68(7)		
	226.28(2)[b]		0.65(4)	≤ 2	0.96		
	229.20(2)		2.62(8)	16.0(8)	3.2(1)		
		230.15(2)	2.64(8)	106(1)	1.35(4)		
	233.51(3)		1.04(7)	15.0(7)	1.12(8)		
	233.85(3)		0.93(7)	9(2)[c]	1.04(12)		
	235.03(3)[b]		0.67(4)	≤ 2	1.0		
	236.62(2)		1.73(6)	12(2)[c]	2.0(1)		
	237.84(3)[b]		0.73(7)	≤ 2	1.15		
	238.16(3)		1.29(8)	16(2)[c]	1.4		
	244.07(3)[b]		0.71(4)	2.5	1.0[d]		
	246.62(5)[b]		0.13(3)	0.25	0.25[d]		
	248.72(3)		2.33(9)	75(1)	2.4(1)		
251.99(<1)			1.37(12)	536(4)	1.37(12)	0.17	1.28(13)
	252.32(5)		0.59(8)	5(1)[c]	0.66(10)		
	253.07(5)		1.03(7)	264(3)	1.04(7)	0.17	1.00(7)
	254.35(5)		0.34(5)	32(5)[c]	0.34(5)		
	255.84(5)[b]		0.77(8)	3.3	1.0[d]		
256.12(<1)			0.70(7)[c]	870(6)	0.70(7)	0.165	0.56(10)
	256.27(5)		1.21(9)	11(1)	1.32(10)		
	257.49(5)		0.20(4)[c]	23(3)	0.20(4)		
257.63(<1)			0.68(15)	1826(7)	0.68(15)	0.165	0.38(21)
	258.42(5)		1.06(7)	13(1)	1.14(9)		
	260.0(1)[b]		0.40(5)	2	0.50[d]		
	260.77(5)		0.79(5)	52(2)	0.80(5)		
	262.61(5)[b]		0.37(4)[c]	≤ 6	0.39		
	263.11(5)		1.37(7)	44(4)[c]	1.42(8)		
	265.30(5)[b]		0.08(4)	0.10	0.50[d]		
	265.94(5)		0.80(6)	56(1)	0.81(6)		
	268.35(5)[b]		0.59(5)	1.5	1.0[d]		
		269.09(5)	1.89(8)	98(1)	0.97(4)		
	273.55(5)[b]		0.25(4)	0.5	0.50[d]		
	276.63(5)[b]		0.54(9)	1.2	1.0[d]		
	277.05(5)		2.77(12)	17.2(8)	3.4(2)		
	278.18(5)		1.01(9)	367(3)	1.01(9)	0.16	0.95(10)
278.93(1)			0.45(7)	225(2)	0.45(7)	0.16	0.41(7)
	280.05(5)		1.27(7)	145(2)	1.28(7)		
	281.85(5)		0.28(6)	15.1(6)	0.28(6)		
	282.74(5)		2.7(2)	175(3)	2.8(2)		
		283.15(5)	1.15(13)	108(1)	0.58(6)		
	285.28(5)[b]		0.42(4)	0.7	1.0[d]		
	288.30(5)[b]		0.64(4)	1.7	1.0[d]		
	290.60(5)		1.30(6)	35(4)[c]	1.35(6)		
291.92(1)			0.70(6)	140(3)	0.71(6)	0.155	0.69(6)
	292.65(5)		1.21(7)	142(3)	1.22(7)		
	294.35(7)		0.62(7)	15(2)[c]	0.65(7)		
	294.75(7)		0.20(6)	9(1)	0.20(7)		
		295.60(7)	0.81(6)	136(2)	0.41(3)		
	297.2(1)		0.12(4)	130(3)	0.12(4)	0.15	0.10(4)
		297.5(1)	0.20(5)	22(2)	0.10(4)		

TABLE II. (*Continued*.)

E_0[a] (keV)							
$s_{1/2}$	$p_{1/2}$	$d_{3/2}$	$g\Gamma_n\Gamma_\gamma/\Gamma$ (eV)	$g\Gamma_n$ (eV)	Γ_γ (eV)	C (10^{-3})	$\Gamma_{\gamma(\mathrm{corr})}$ (eV)
	299.80(7)[b]		0.40(5)[c]	2	0.50[d]		
		300.40(7)	1.44(7)	52(1)	0.74(4)		
		302.11(5)	2.13(7)	16(2)	1.23(5)		
	306.6(1)		1.46(9)	400(4)	1.47(9)	0.15	1.4(1)
		307.36(5)	3.10(11)	210(1)	1.57(6)		
	308.7(1)		0.75(8)[c]	3	1.0[d]		
	311.3(1)		0.60(8)	12.7(7)	0.61(9)		
	313.5(1)		2.26(13)	10(2)[c]	2.9(2)		
317.02(<1)			1.5(2)[c]	2788(9)	1.5(2)	0.15	1.1(3)
	317.2(1)[b]		2.8(1)	≤12	3.6		
	321.5(1)		1.22(12)	20(5)[c]	1.3(1)		
	322.8(1)		1.01(10)	5.2(5)	1.25(14)		
	324.6(1)[b]		0.67(10)	2	1.0[d]		
325.52(<1)			2.5(5)[c]	7084(17)	2.5(5)	0.14	1.5(7)
	326.5(1)[b]		0.75(8)[c]	3	1.0[d]		
		327.4(1)	2.7(1)	16(1)	1.6(1)		
	329.0(1)		0.94(11)	40(2)	0.96(11)		
	329.6(1)[b]		0.69(7)[c]	2.2	1.0[d]		
	331.1(1)[b]		0.57(4)[c]	1.3	1.0[d]		
	334.1(1)		1.2(1)	230(2)	1.2(1)		
		336.1(1)	2.2(1)	162(3)	1.12(5)		
338.48(<1)			3.0(5)[c]	3563(14)	3.0(5)	0.13	2.5(6)
	338.9(1)[b]		0.41(7)	≤7	0.44		
	341.4(1)		1.00(10)	105(3)	1.01(10)		
	342.7(1)		0.20(3)[c]	110(10)[c]	0.20(3)		
	343.1(1)		1.01(12)	210(4)	1.01(12)		
	344.1(1)[b]		1.49(10)	4	2.5[d]		
	345.4(1)[b]		0.86(8)[c]	2	1.5[d]		
	348.17(1)		5.2(2)	94(3)	5.5(2)		
	349.1(1)		2.3(1)	27(1)	2.6(2)		
		350.0(1)	1.5(1)	20(5)[c]	0.81(8)		
		352.37(7)	1.62(10)	9(3)[c]	1.0(1)		
		354.27(10)	1.82(13)	493(4)	0.91(6)	0.13	0.87(6)
		355.4(1)	1.14(8)	30(10)[c]	0.60(6)		
357.65(<1)			3.0(5)[c]	1619(10)	3.0(5)	0.13	2.8(5)
	358.7(1)[b]		1.34(12)	10	1.5[d]		
		359.3(1)	2.0(2)[c]	1256(7)	1.0(1)	0.13	0.9(1)
	361.1(1)[b]		0.88(13)	7	1.0[d]		
	365.6(1)		0.8(2)	60(5)[c]	0.8(2)		
		366.1(1)	3.7(2)	15(2)[c]	2.5(2)		
	369.7(1)[b]		1.22(11)	≤7	1.5		
		370.48(1)	1.37(11)	56(15)[c]	0.7(1)		
		371.68(1)[b]	3.1(2)	6.5	3.0[d]		
	373.4(1)		0.17(11)	30(5)[c]	0.18(11)		
	374.6(1)[b]		0.37(3)[c]	1.4	0.50[d]		
	376.8(1)[b]		1.39(11)	7	1.6[d]		
376.84(<1)			3.5(5)[c]	3865(18)	3.5(5)	0.13	3.0(6)
	378.0(2)[b]		0.45(10)	4.5	0.50[d]		
	379.4(1)		2.7(2)	478(7)	2.7(2)	0.13	2.6(2)
	381.1(1)		2.07(13)	30(2)	2.22(15)		
	381.8(1)[b]		2.6(2)	≤10	3.5		
383.13(5)			1.86(13)	370(5)	1.87(13)	0.13	1.82(13)
	386.2(1)[b]		1.85(11)	≤5	2.9		
		388.2(1)	0.78(13)	260(5)	0.39(6)	0.13	0.37(6)
	388.8(1)		2.82(13)	160(5)	2.88(13)		

TABLE II. (*Continued.*)

E_0[a] (keV) $s_{1/2}$	$p_{1/2}$	$d_{3/2}$	$g\Gamma_n\Gamma_\gamma/\Gamma$ (eV)	$g\Gamma_n$ (eV)	Γ_γ (eV)	C (10^{-3})	$\Gamma_{\gamma(\mathrm{corr})}$ (eV)
		393.0(1)	1.60(11)	375(5)	0.80(6)	0.13	0.78(6)
	394.8(1)[b]		0.48(9)	0.9	1.0[d]		
	397.0(1)[b]		0.57(7)	1.3	1.0[d]		
		398.1(1)	0.40(14)	460(4)	0.20(7)	0.12	0.17(7)
	399.2(1)		1.27(11)	40(6)[c]	1.38(13)		
	401.0(1)[b]		0.43(10)	3	0.50[d]		
	401.6(1)[b]		0.54(8)	5.4	0.60[d]		
		402.8(1)	3.3(2)	443(5)	1.65(8)		
	404.0(1)[b]		1.10(11)	4	1.5[d]		
	407.9(1)		1.4(3)	30(6)[c]	1.5(3)		
	408.3(1)		0.8(2)	15(5)[c]	0.9(3)		
		409.9(1)	0.6(3)	220(5)	0.30(14)		
	410.2(1)		1.0(3)	13(1)	1.1(3)		
413.44(5)			0.97(14)	344(6)	0.97(15)	0.12	0.93(15)
		415.4(1)	1.5(3)	400(6)	0.77(16)	0.12	0.75(16)
		415.7(1)	2.3(3)	34(3)	1.2(2)		
418.3(1)			1.28(10)	68(3)	1.30(11)		
	419.9(1)		2.29(12)	20(5)[c]	2.6(2)		
422.49(<1)			2.3(3)[c]	1861(15)	2.3(3)	0.12	2.1(3)
		424.6(1)	2.32(12)	70(14)[c]	1.20(7)		
	426.1(1)[b]		0.84(8)	5	1.0[d]		
	427.0(1)[b]		1.5(2)[c]	10	1.75[d]		
	429.1(1)		0.7(2)	600(10)	0.7(2)	0.12	0.6(2)
		429.9(1)	1.84(14)	27(2)	0.99(8)		
	431.9(1)		1.3(2)	240(10)	1.3(2)		
		432.4(1)	1.2(2)	180(8)	0.63(8)		
		435.3(2)	0.6(2)	510(5)	0.31(9)	0.12	0.28(9)
	436.5(2)[b]		0.43(15)[c]	3	0.50[d]		
437.73(1)			1.5(3)[c]	1219(4)	1.5(3)	0.12	1.35(30)
		438.9(1)	3.1(2)	30(6)[c]	1.72(12)		
		440.9(1)	3.3(2)	180(5)	1.68(10)		
443.9(2)			2.0(2)	177(7)	2.0(2)		
	444.4(2)[b]		1.0(2)[c]	3	1.5[d]		
	445.5(2)		0.25(5)[c]	95(4)	0.25(5)		
	447.1(2)[b]		0.5(2)	1.0	1.0[d]		
448.00(1)			2.0(5)	2733(36)	2.0(5)	0.12	1.7(5)
	448.9(1)		1.7(2)	24(2)	1.8(2)		
		451.2(1)	1.9(2)	150(10)	0.95(9)		
454.19(7)				788(80)			
463.5(1)				1600(200)			
485.9(1)				3100(400)			
498.6(1)				3400(400)			
522.2(1)				3600(500)			
527.0(1)				2800(300)			
540(2)				79 000(1000)			
555(3)				1700(200)			

[a]Resonance energy after all corrections discussed in Sec. VI were applied. Within parentheses are statistical uncertainties. The notation is such that $-0.15(11)$ stands for -0.15 ± 0.11. The same notation is used elsewhere in the table. See Sec. III for explanation of spin assignments.

[b]Resonance seen in capture only. If an upper bound of $g\Gamma_n$ is given, it is clearly seen as such on the theoretical fit to the transmission data and must be kept associated with the corresponding value of Γ_γ.

[c]Parameter adjusted by trial and error. The uncertainty was estimated from the sensitivity of the fit to the variation of this parameter.

[d]Assigned value of Γ_γ (see Sec. III for details).

[e]Resonance seen in transmission only.

fitting the data up to 550 keV were anticipated. However, a satisfactory fit to the data up to 500 keV was obtained because the three s-wave resonances at 522, 527, and 555 keV acted as fictitious resonances in addition to the large one which, in the process of fitting this region, moved from 540 to 567 keV. Too many constraints were built in the system and a fit to the 500- to 550-keV region could not be achieved. More than one resonance above the range of energy to be analyzed is probably necessary. In view of this problem and since the capture data were not analyzed above 452 keV, it was decided to limit the transmission data analysis also at 452 keV. The final set of resonance parameters is reported in Table II. In addition to the large resonance at 540 keV, the seven s-wave resonances given above 452 keV also contribute to the calculated theoretical transmission below 452 keV and must be kept as part of the parameter file obtained from the analysis of the transmission data from 1 to 452 keV. Calculations were performed with fictitious $l=1$ and $l=2$ resonances; however, due to penetrabilities, they did not contribute to the smooth background. Only the four resonances seen in the transmission data above 450 keV were slightly affected. Therefore, our final parameter file contains 257 resonances between 1 and 452 keV, two negative energy resonances, and eight fictitious s-wave resonances above 452 keV.

IV. CAPTURE MEASUREMENTS

Neutron capture measurements made from 2.5 keV to ~5 MeV were based on 4.955- and 49.11-g enriched metal samples containing 99.79% ^{60}Ni. While the capture yield depends primarily on weight and purity, the resonance self-protection and multiple-scattering corrections depend on the dimensions of the samples which were approximately 26 mm by 52 mm with a thickness of 0.50 mm for one and 4.65 mm for the other. These thicknesses correspond to 0.003 68 and 0.0372 atoms/barn, respectively.

The samples were exposed to the collimated ORELA neutron flux at 40.12 m from the electron target and moderator. Capture gamma rays were detected by a pair of C_6F_6-based liquid scintillators, one on each side of the sample, outside the beam. Accelerator conditions were 1000 pulses of 4 ns each per second and an average power of 7 kW. The run was completed in 78 h with partial results recorded four times during the run for consistency checks. The time resolution of the scintillation detectors and associated electronics, as determined with coincident ^{60}Co gamma rays, was 2.1 ns FWHM. More important at most energies was the neutron slowing-down time in the moderator. Expressed as an equivalent spread in flight path, this was found to be about 28 mm FWHM by fitting the narrowest resonances below 20 keV.

The total gamma-ray energy emitted as a function of neutron time-of-flight was derived by pulse-height weighting[11] and was corrected for a calculated 2.0% energy loss in the thin sample and 12.4% in the thick sample. The neutron flux was monitored by a 0.5-mm ^{6}Li glass scintillator[12] located 0.4 m upstream from the sample position. Above 70 keV this monitor had been calibrated against a ^{235}U fission chamber.[13] The capture efficiency was calibrated at 4.9 eV with a 50-μm gold foil sample using the saturated resonance technique.[14]

The raw capture data were corrected for electronic deadtime losses, amplifier gain standardization, environmental backgrounds, average scattered-beam background, and the excitation energy reached in ^{61}Ni. The time-of-flight data were rebinned to a set of neutron-energy scales, and the capture yield was expressed as millibarns per nucleus of ^{60}Ni in the target. The estimated various systematic uncertainties reported in Table III give a global systematic uncertainty of 3.4% to 4% on the capture yield in the range of energy analyzed in this report.

V. CAPTURE DATA ANALYSIS

The capture data have been analyzed with a least-squares fitting program[15] LSFIT using the Breit-Wigner formula

$$\sigma_{n\gamma}=\pi k^{-2}\frac{g\Gamma_n\Gamma_\gamma}{(E-E_c)^2+(\Gamma/2)^2}\ , \tag{5.1}$$

where g is the statistical weight factor, Γ_n, Γ_γ, and Γ are the neutron, radiation, and total width, respectively, for each resonance, and E_c is the resonance energy.

A field, encompassing up to 500 data points and up to 16 resonances, is analyzed at one time. The program iterates upon trial parameters applying corrections for systems resolution, Doppler width, resonance self-protection, and multiple scattering.

Analysis of the thin sample data was conducted from 2.5 to 82 keV. The thick sample data were analyzed starting at 32 keV and up to 452 keV. The capture kernels reported in Table II are from the analysis of the thin sample data up to 50 keV and from the thick sample data at higher energies. Although resonance structure was observed well above the inelastic threshold of 1355 keV, the complexity of the spectrum and the increasing uncertainty in

TABLE III. Systematic uncertainties on the capture yield in percent.

Saturated resonance calibration	3
Shape of the ^{6}Li(n,α) cross section at 50 keV	1
Shape of the ^{6}Li(n,α) cross section at 250 keV	2
Shape of the ^{6}Li(n,α) cross section at $E_n \geq 500$ keV	3
Pulse height weighting technique	1
Gamma-ray self-absorption of thin sample	0.4
Gamma-ray self-absorption of thick sample	1.0
Detector bias extrapolation ($E_{\text{bias}}=153$ keV)	0.4
Misalignment of sample or neutron beam	<0.2
Uncertainty in detector efficiency from gain drifts of electronics	<0.4

matching resonances in capture data with resonances in transmission data (see Sec. VI) made analysis of single resonances unrealistic above 450 keV.

If a resonance has not been previously seen and analyzed in the transmission data, the neutron width Γ_n is not known and only the capture area

$$A_\gamma=(2\pi^2/k^2)(g\Gamma_n\Gamma_\gamma/\Gamma)$$

is determined. About 30% more resonances are seen in capture than in transmission. Therefore, after the capture data analysis was completed, we went back to the transmission data. Knowing from the capture analysis what the resonance energy is, it becomes possible to adjust the neutron width to a reasonable value which would show a small resonance on the theoretical curve fitting the transmission data where there was none before. These small resonances in transmission are smaller than the statistical spread of the data points, and for some of them the neutron widths given in Table II are the maximum acceptable values.

The parameters of the overlapping resonances were not all adjusted by the code simultaneously but were adjusted separately in successive runs until the best set of parameters was obtained which would give the most satisfactory fit to the capture and transmission data simultaneously.

Since these data showed a small low-energy (i.e., time delayed) tail on the usual Gaussian resolution function, a resolution shape modification is included in the code. The fraction of the neutrons which showed an asymmetric resolution function was 10% at 5 keV increasing up to 40% for 145 keV neutrons. The asymmetric part is convoluted with a negative exponential whose time constant is given as a fraction of the Gaussian resolution (FWHM). Here the decay constant is 68% of the resolution.

In order to evaluate properly the part of the multiple scattering due to the attenuation of the neutron flux in the sample, one needs to know the off-resonance scattering cross section σ_{off} in the region of each resonance. For s-wave resonances and for $l>0$ resonances not on top of s-wave resonances, σ_{off} is equal to the effective potential scattering which decreases smoothly from 8 to 3 b as the neutron energy increases from 12 to 450 keV. At low energy (below 100 keV) for resonances which are on top of large s-wave resonances, σ_{off} can vary drastically. For example, for the $l>0$ resonances at 12.220 and 13.264 keV on top of the large 12.487-keV s-wave resonance, σ_{off} is as large as 200 b and 120 b, respectively. These resonances, as well as the $l>0$ resonances at 28.497, 29.480, and 65.573 keV, have been analyzed individually using the proper σ_{off} given by the transmission data and taking as background the capture cross section of the s-wave resonance at the corresponding energy.

A background term having a $E^{-1/2}$ energy dependence can be adjusted by the code if necessary. This background term includes the direct capture, if any, and the capture in the tails of the faraway s-wave resonances as well as the incompletely subtracted background from various sources. For these ^{60}Ni capture data, the optimum background for good fits to well-isolated resonances appeared to be roughly uniform—about 5 ± 2 mb up to 50 keV where the data taken with the thin sample (0.003 68 atoms/barn) were analyzed, and 2.5 ± 1 mb for the thick sample data above 50 keV. The optimum value of the background can be checked on a few well-separated individual resonances up to 250 keV. At higher energy, the overlap of the resonances does not permit picking up the background between the resonances. Satisfactory fits were obtained using the uniform value of 2.5 mb found earlier, but above 250 keV a 2-mb uncertainty on the background is more realistic. Figures 1 to 7 show the capture data before the background corrections were applied, whereas these background corrections have been

subtracted from the capture data shown in Figs. 8 to 11.

A correction for the capture in the detector environment of neutrons scattered from discrete resonances in the sample is required.[16] This prompt neutron sensitivity can be formulated as a correction to Γ_γ such that

$$\Gamma_{\gamma(\mathrm{corr})}=\Gamma_\gamma-C\Gamma_n\ , \tag{5.2}$$

where C is dependent on the amount and distribution of absorber in the vicinity of the detector. This correction factor is energy dependent and varies from 10^{-3} to 10^{-4} over the energy range of this analysis as shown in Fig. 12. Values of C are considered accurate to $\sim 50\%$. This correction has been applied and C is given in Table II if $C\Gamma_n$ is 3% or more of Γ_γ. Below 200 keV, this correction is responsible for most of the uncertainty in the capture width of large s-wave resonances where $C\Gamma_n$ can be as large as half of the capture width given by the code.

VI. ENERGY SCALE CALIBRATION

The energy of a resonance, E_T, seen in the transmission data is systematically larger than the energy E_c of the corresponding resonance seen in the capture data. The differences between the two energy scales, E_T-E_c, increases smoothly from 0.01% of the neutron-incident energy at 20 keV to 0.06% of the neutron-incident energy at 250 keV. When the resonances are well separated in both sets of data, it is possible to match them with good confidence. This is true up to 250 keV, as shown in Figs.

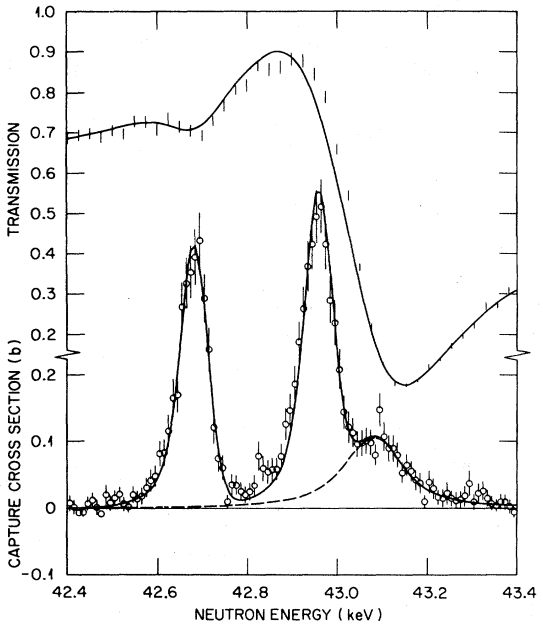

FIG. 8. Fits to the transmission and capture data in the region of the 43.1-keV s-wave resonance. The dashed curve is the s-wave resonance contribution to the capture cross section.

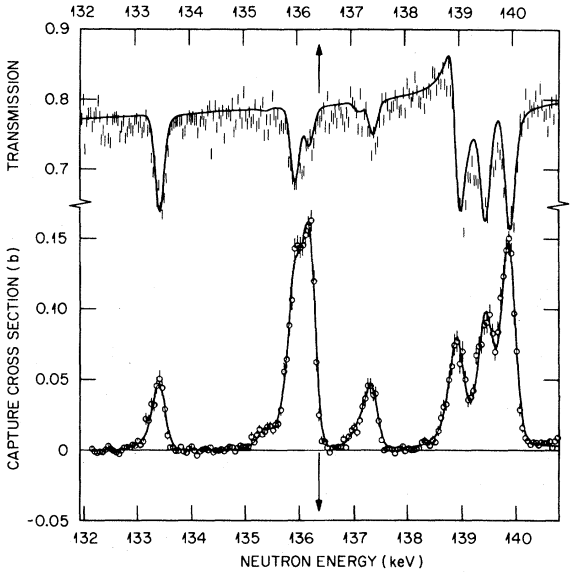

FIG. 9. Fits to the transmission and capture data in the 132- to 141-keV region. The shift between the two energy scales corresponds to the correction (E_T-E_c) discussed in Sec. VI.

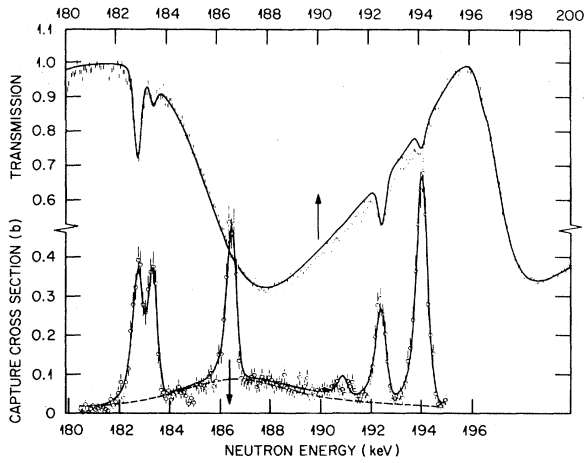

FIG. 10. Fits to the transmission and capture data in the region of the strong s-wave resonance at 186.51 keV. The dashed curve is the s-wave resonance contribution to the capture cross section. The shift between the two energy scales corresponds to the correction (E_T-E_c) discussed in Sec. VI.

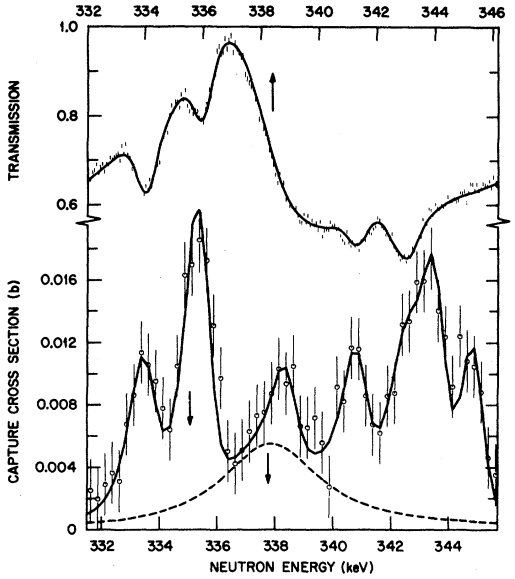

FIG. 11. Fits to the transmission and capture data in the 332- to 346-keV energy region. The dashed curve is the s-wave resonance contribution to the capture cross section. The shift between the two energy scales corresponds to the correction $(E_T - E_c)$ discussed in Sec. VI.

2 to 5, and in more detail in Figs. 9 and 10. Above 250 keV, the resonances in the transmission data are still fairly well separated but the resonances in the capture data become progressively more overlapping. We start having difficulty in matching the resonances around 300 keV. We were able to get fits similar to the ones shown in Fig. 11 only with a sharp increase in the difference between the two energy scales (0.14% of the neutron-incident energy at 340 keV). The uncertainty on the shift between the two energy scales, $\Delta(E_T - E_c)$, is about 0.01% of the neutron incident energy below 300 keV and 0.05% above 300 keV. Here we need to stress the point that, especially above 300 keV, we do not claim that the fits and the corresponding set of resonance parameters are in any way unique. We probably could obtain satisfactory fits as well with a slightly different energy shift but we would need more resonances to fit the same data.

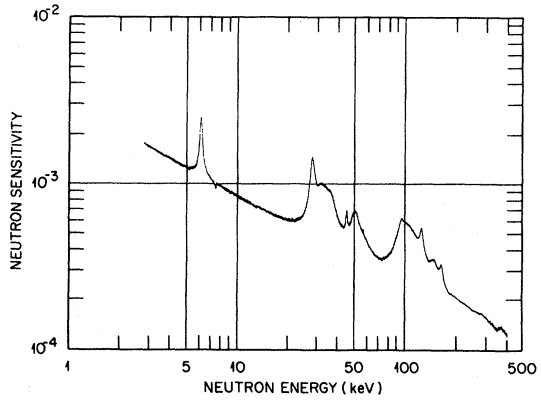

FIG. 12. Detector neutron sensitivity as a function of the incident neutron energy for the ^{60}Ni targets.

The resolutions in both experiments are nearly the same and cannot justify the choice of one energy scale over the other. Typical values of the resolution are given in Table I. Below 60 keV, the transmission data analyzed are the data using the ^{6}Li glass detector with a burst width of 40 ns which explains the larger resolution of the transmission in this energy region.

A high resolution transmission experiment on a natural nickel target (200-m flight path, 8-ns burst width) is reported in Ref. 17. Based on the comparison of the energies of six ^{60}Ni resonances in both transmission data sets, the energy scale of the ^{60}Ni transmission data is found to be systematically lower than the energy scale of the natural nickel transmission data by 0.033%. Also, the energies of four sulfur resonances seen in the transmission spectrum of the open beam (due to the sulfur content of the filter) are systematically lower than the energies of the corresponding resonances of Refs. 18 and 19 by 0.037%. A normalization factor of 0.035 $\pm$0.015% of the neutron incident energy was applied to the resonance energies of the transmission data, E_T, to obtain the energy parameters E_0 of Table II. Since this normalization factor is independent of the energy, it should be associated only with a correction to the flight path length of 14 mm $\pm$6 mm (see Ref. 2 for more details).

Recent Monte Carlo calculations of the ORELA moderator time distribution vs neutron energy[20] are in good agreement with this possible shift in the flight path since it indicates a correction of 10 mm at 10 keV, rising to 29 mm at 400 keV for ^{60}Ni transmission data which used only the moderated flux.

The cumulative corrections $E_0 - E_c$ applied on the energy scale of the capture data are energy dependent and therefore could be associated to shifts in both the flight path and the time of flight of the capture experiment of 4 ± 3 mm and -2.1 ± 0.3 ns, respectively.

The Monte Carlo calculations of moderation time for ORELA (Ref. 20) reproduce quite closely the observed slope of $(E_T - E_c)$ in percent of the incident energy up to 250 keV. However, this slope disagrees with the calculations by two standard deviations at 400—450 keV. This suggests that there

may be misidentifications of capture peaks with resonances seen in transmission above 300 keV.

VII. RESULTS AND DISCUSSIONS OF THE UNCERTAINTIES

A. Resonance parameters and fits

The final resonance parameters obtained in the combined analyses of the ^{60}Ni transmission and capture data from 1 to 452 keV are given in Table II. Well-separated resonances are spaced by one blank line, strongly overlapping resonances are grouped, and resonances forming a multiplet are grouped and joined by a bracket. There is not a clear distinction between what is called "strongly overlapping" resonances and what is called a "multiplet"; therefore, this classification should not be taken too seriously. Nevertheless, it was adopted since we found it useful in spotting at a glance a group of resonances on the plots and the corresponding group of parameters in Table II. The first two and the last eight resonances in this table are fictitious resonances.

The resonance energy, E_0, reported in the first three columns is the corrected neutron energy as discussed in Sec. VI. Within parentheses are the statistical uncertainties.

The capture kernels and neutron widths are given in the next two columns. Within parentheses are the statistical uncertainties except if the superscript c is used. The capture kernel is the only well-known parameter associated with the 89 resonances seen only in the capture data. However, the neutron and radiation widths of these resonances are not totally arbitrary. Estimated values of these parameters are given but without uncertainty.

The radiation widths reported in the sixth column are defined only for resonances seen in both sets of data with the exception of the resonance at 2.253 keV. This small resonance, analyzed only in transmission because our capture data does not go below 2.5 keV, is best fitted with the set of parameters reported in Table II.

The correction factor C for the neutron sensitivity of the detector and the corrected radiation widths $\Gamma_{\gamma(\mathrm{corr})}$ are shown in the next two columns. The uncertainties associated with the corrected radiation widths are the quadratic combination of the 50% uncertainty on the correction factor C with the statistical uncertainties on Γ_γ.

In Figs. 1 to 7 the transmission and capture data are shown, and the transmission data are compared to the theoretical transmission calculated with all the resonance parameters given in Table II. The fits to both kinds of data are shown in detail in Figs. 8 to 11 for four small energy regions. The theoretical transmission is the same as in Figs. 1 to 7. The fits to the capture data are typical of the fits obtained in the other energy regions. The top (E_T) and bottom (E_c) energy scales have been shifted by the proper correction ($E_T - E_c$) as discussed in Sec. VI, so that the resonances seen in both sets of data are aligned. Around 40 keV (Fig. 8), the correction is too small to be seen (less than 10 eV). The shift in Fig. 9 is 50 eV and 90 eV in Fig. 10. It jumps to approximately 0.5 keV around 340 keV (Fig. 11). The dashed lines in Figs. 8, 10, and 11 are the capture cross-section contributions of the large s-wave resonances present in these regions.

B. Estimated uncertainties and their correlations

The search codes give the statistical uncertainties and their correlations. The correlation matrix given by the code SAMMY at the end of the procedure described in Sec. III gives the correlations between the statistical uncertainties of all the 203 adjusted parameters inside and outside of the 1- to 452-keV energy range, whereas the correlation matrices for the parameters obtained in the capture analysis are relevant only to small energy regions as shown in Figs. 8 to 11.

For conciseness, "correlations between parameters" will be used from now on instead of "correlations between statistical uncertainties of parameters" when this simplification does not lead to confusion.

1. Resonance energies

The statistical uncertainties on the energies of the s-wave resonances given in Table II were determined by the code SAMMY from the transmission data analysis except for the three narrow resonances at 200.59, 418.3, and 443.9 keV which were better defined in the capture data. The systematic uncertainty of 0.015% on the renormalization of the energy scale discussed in Sec. VI is the main source of uncertainty on the energies of the s-wave resonances as illustrated in Table IV. The contribution to the covariance due to the statistical uncertainties given by the code SAMMY will always be negligible compared to the contribution from the systematic uncertainties which are dominant and 100% correlated.

The statistical uncertainties on the energies of all the other resonances are obtained mostly from the LSFIT code used in the fitting of the capture data.

TABLE IV. Sample of uncertainties on the final energy parameter E_0. E_T and E_c stand for the energy of resonances in the transmission and capture data, respectively.

E_0 (keV)	l	ΔE_T or ΔE_c statistical (eV)	Systematic $\Delta(E_T-E_c)$ (eV)	Systematic $\Delta(E_0-E_T)$ 0.015% of E_0 (eV)	ΔE_0 (eV)
12.487	0	1		2	2.2
13.624	>0	1	1.4	2	2.6
65.228	0	1		10	10
65.573	>0	2	5	10	11
139.03	0	<10		21	21
139.56	>0	20	15	21	33
186.51	0	<10		29	29
192.59	>0	20	23	29	42
251.99	0	<10		38	38
252.32	>0	50	30	38	63
422.49	0	<10		64	64
424.6	>0	100	200	64	233

Some energies of very small or very strongly overlapping resonances were adjusted by trial and error. In addition to the statistical uncertainties given in Table II, the two sources of systematic uncertainties discussed in Sec. VI must be considered. Final estimated uncertainties on E_0 are given in Table IV for six $l>0$ resonances. This shows that up to 300 keV the three sources of uncertainties contribute about equally to ΔE_0, but above 300 keV the large uncertainty on the shift between the two energy scales, E_T-E_c, is the dominant factor.

The energy parameters of $l>0$ resonances are correlated only in the case of strongly overlapping resonances. Take, for example, the doublet in Fig. 10. The energies of the resonances are 194.19 and 194.54 keV with statistical uncertainties of 10 and 30 eV, respectively. The correlation between these uncertainties is 0.26. The systematic uncertainties are 23 eV for $\Delta(E_T-E_c)$ and 29 eV for $\Delta(E_0-E_T)$, similar to what is given in Table IV for the resonance at 192.59 keV. Therefore, the covariance of the energy parameters due to the statistical uncertainties is 78 eV^2 compared to 1370 eV^2 for the covariance due to the fully correlated systematic uncertainties. It can be seen that even for a doublet the contribution to the covariance of the energy parameters due to the statistical uncertainties is negligible.

2. Neutron widths

Since the systematic uncertainties in the transmission experiment were not parametrized, they could not be included in the SAMMY input. Therefore, an estimate of the systematic uncertainties on the neutron widths cannot be given. The various sources of systematic uncertainties on fluorine transmission measurements were investigated and reported in Ref. 4. A similar investigation on ^{60}Ni transmission measurements led to an estimated 2% systematic uncertainty. This 2% systematic uncertainty should be added to the statistical uncertainties of cross sections calculated with the resonance parameters given in this report.

In the transmission data, most s-wave resonances are well separated. The largest correlation coefficient between the neutron widths of two s-wave resonances is -0.36 which will, most certainly, give covariance contributions negligible compared to the ones due to the systematic uncertainties.

Covariances due to statistical uncertainties on the neutron widths of an $l>0$ resonance on top of an s-wave resonance or on $l>0$ resonances forming a doublet are also quite small even when the correlation coefficient is as large as 0.7. This is because the statistical uncertainties are small due to the large number of data points.

3. Capture kernel

A systematic uncertainty on the capture yield of 3.4—4% was reported in Sec. IV. An additional systematic uncertainty of 0.5% is associated with the multiple scattering and self-protection corrections in the data reduction.[21] Finally, two sources of systematic uncertainty arise from the data analysis. One is related to the fitting of the shape of the reso-

TABLE V. Uncertainties on the capture kernel K ($K=g\Gamma_n\Gamma_\gamma/\Gamma$).

E_0 (keV)	K (eV)	$\Delta K/K$ statistical (%)	$\Delta K/K$ systematic (%) Sys. 1	Sys. 2	Total sys.
21.274	0.022	10	4.6	2.7	5.3
23.788	0.24	4	4.6	0.3	4.6
136.03	1.34	4	5.0	0.9	5.1
226.28	0.65	6	5.0	7.5	9
341.4	1.0	10	5.0	25	26
431.9	1.3	15	5.0	20	21
432.4	1.2	17	5.0	20	21

nances by the code. This uncertainty is hard to estimate. The shape of a resonance is affected by the spin assignment and by the energy resolution. In Ref. 21 this uncertainty is estimated to be less than 3%. All these uncertainties, when combined, add up to 4.6% below 100 keV and 5% above 100 keV. Examples of these relative uncertainties are shown in the fourth column of Table V (Sys. 1). The other source of systematic uncertainty associated with the data analysis is in the subtraction of the background discussed in Sec. V which is the main source of systematic uncertainty above 250 keV and for resonances with small capture kernel. Examples of these relative systematic uncertainties are given in the fifth column of Table V (Sys. 2).

Some systematic uncertainties discussed above apply only to narrow resonances. The 3% maximum contribution to the systematic uncertainty from the finite resolution and the lack of knowledge of the spin of the resonances does not apply to large s-wave resonances. On the other hand, the relative uncertainty associated with the multiple scattering and self-protection corrections can be as much as 5% (compared to an estimated 0.5% for narrow resonances). Also, for large s-wave resonances, even at low energy the subtraction of the background during the analysis is a major source of systematic uncertainty.

As an example of the final correlation between the uncertainties on the capture kernels of two strongly overlapping resonances, we chose two resonances for which the neutron widths are much larger than the capture kernels. For such resonances the correlation coefficient between the radiation widths (given by the code LSFIT) is the same as the correlation coefficient between the capture kernels. Let us consider the two following resonances:

$$E_{0_1}=431.9 \text{ keV}, \quad K_1=1.3\pm0.2 \text{ eV},$$

$$g\Gamma_{n_1}=240\pm10 \text{ eV};$$

$$E_{0_2}=432.4 \text{ keV}, \quad K_2=1.2\pm0.2 \text{ eV},$$

$$g\Gamma_{n_2}=180\pm8 \text{ eV},$$

where K denotes the capture kernel $g\Gamma_n\Gamma_\gamma/\Gamma$. The correlation coefficient between the statistical uncertainties of K_1 and K_2 is -0.88. Consequently, the statistical contribution to the covariance of K_1 and K_2 is equal to -0.035 eV^2. The relative systematic uncertainties are 21% for K_1 and K_2 (Table V) and are fully correlated. Therefore the systematic contribution to the covariance is 0.068 eV^2. Since the two contributions are of opposite signs, the total covariance $\langle dK_1,dK_2\rangle$ is equal to $+0.033$ eV^2. By definition, the correlation coefficient $C(K_1,K_2)$ is given by

$$C(K_1,K_2)=\frac{\langle dK_1 dK_2\rangle}{(\langle dK_1{}^2\rangle\langle dK_2{}^2\rangle)^{1/2}}, \tag{7.1}$$

where $\langle dK_1{}^2\rangle$ and $\langle dK_2{}^2\rangle$ are the variances of the capture kernels. The final correlation coefficient for these resonances is $+0.31$. This illustrates that the combined effect of the statistical and systematic uncertainties should be carefully studied before drawing a conclusion on the final correlation coefficient.

VIII. COMPARISON WITH OTHER WORKS

The results of this analysis are compared with the Harwell transmission analysis by Syme *et al.*[22] and with the Karlsruhe capture analysis of Fröhner.[23] Both analyses were reported in 1977. Also given for

comparison are the resonance parameters of Stieglitz *et al.*[24] which were the main source of data used in the ENDF evaluations. Reference 2 should be consulted for more details and for a complete listing of references of previous publications on ^{60}Ni resonance parameters.

In Table VI, parameters for *s*-wave resonances are compared up to 200 keV with values given in earlier publications. Resonance energies are generally in good agreement with Ref. 24 but systematically higher than the two other works.[22,23] (Above 150 keV, the discrepancies with the energy parameters of Fröhner[23] are as large as 2 keV.) The neutron widths are in better agreement with Ref. 22 than with Ref. 24 for the first five *s*-wave resonances (up to 90 keV). Between 100 and 200 keV it is the reverse. The radiation widths of the first two *s*-wave resonances at 12.487 and 28.709 keV are in good agreement with the values reported by Fröhner because in this low-energy region the *p*-wave resonances on top of these two *s*-wave resonances are resolved in Fröhner's analysis as well as here. All other radiation widths for *s*-wave resonances reported in earlier publications are larger than the values obtained from this analysis. As illustrated by the first two examples in Table VII, around 43 and 65 keV, the unresolved $l>0$ resonances on top of the *s*-wave resonances are responsible for these discrepancies. In each case two large $l>0$ resonances were included in the *s*-wave resonance capture area reported in earlier works. Figure 8 illustrates how well these resonances are separated in the ORELA capture data in the 43-keV region.

The level density of the $l>0$ resonances in this transmission data analysis is three times higher than in Ref. 22. Also, these new ORELA capture data made possible the separation of many levels which could not be resolved before. Since a detailed comparison of our resonance parameters of the $l>0$ resonances with previously published results would be too cumbersome, comparison was made only between the capture kernels of resonances below 40 keV (Table VIII) and for a small energy region between 132 and 140 keV. In Table VIII the capture kernels reported by Stieglitz *et al.* for the two first resonances at 2.25 and 5.53 keV are higher than our values but almost within the uncertainties. For the two resonances at 12.22 and 13.62 keV, which are on top of a large *s*-wave resonance, the capture kernels found in this analysis are in good agreement with the values reported by Fröhner but are in complete disagreement with the reported values of Stieglitz. No resonance around 17 keV (reported by Fröhner) could be seen either in our transmission or in our capture data obtained with the thick or the thin sample. Above 23 keV our values are systematically

TABLE VI. ^{60}Ni *s*-wave resonance parameters compared to other works up to 200 keV.

Present work			Syme *et al.*, Ref. 22		Fröhner, Ref. 23		Stieglitz *et al.*, Ref. 24		
E_n (keV)	Γ_n (eV)	Γ_γ (eV)	E_n (keV)	Γ_n (eV)	E_n (keV)	Γ_γ (eV)	E_n (keV)	Γ_n (eV)	Γ_γ (eV)
12.487(1)	2358(3)	2.6(9)	12.22(5)	2354(1)	12.3(2)	2.7(5)	12.47(6)	2660(100)	3.3(3)
28.709(1)	698(1)	0.7(5)	28.650(1)	681.6(2)	28.64(10)	0.60(15)	28.64(10)	800(50)	1.10(10)
43.105(1)	104.4(6)	0.20(4)	43.050(4)	84.1(1)	42.92(11)	0.98(16)	43.08(23)	77(15)	1.73(18)
65.228(1)	443.0(8)	0.94(9)	65.11(2)	459.9(8)	65.12(16)	1.9(3)	65.13(40)	390(30)	2.43(25)
86.837(1)	398(1)	0.62(10)	86.667(7)	341(2)	86.35(22)	1.5(3)	86.8(6)	330(25)	
98.085(1)	1002(2)	0.9(3)	97.85(1)	835.6(2)	96.79(30)	1.20(25)	98.1(7)	870(70)	
107.85(1)	649(1)	0.8(2)	107.479(4)	265.3(5)	107.77(30)	1.35(25)	107.8(8)	610(60)	
139.03(1)	30.7(5)	1.18(6)							
156.36(1)	472(1)	0.35(13)	~156	~100	154.8(7)	0.70(12)	156.4(12)	440(50)	
161.74(1)	1325(2)	0.46(25)	161.41(2)	1010(1)	160.9(9)	2.2(4)	162.1(13)	1250(130)	
186.51(1)	5237(6)	2.9(8)	185.41(11)	9150(2)	184.0(15)	3.2(8)	186.5(15)	6000(800)	
197.64(1)	3025(2)	1.2(4)	197.03(5)	3692(2)	195.0(20)	4.1(10)	198.0(18)	3100(350)	

higher than those of Fröhner. In the 132- to 140-keV region (see Fig. 9), neither the resonances at 133.52 keV nor the doublet around 137.4 keV were seen in any other total cross section or capture measurements, even though Syme *et al.*[22] claim a better energy resolution (0.075 ns/m) than the one obtained at ORELA in this transmission experiment (0.13 ns/m). Around 136 keV, the small resonance followed by the two large overlapping resonances were seen, in earlier publications, as a single resonance in capture data and not at all in any total cross-section measurements. It is shown in Table VII that the sum of the capture kernels of the three resonances reported in this work is equal to the capture kernel given by Fröhner; and smaller but in the range of the possible values given by Stieglitz *et al.* Even the three resonances around 139 keV which are separated by half a keV were not resolved before. In the present work, these three resonances are fairly well separated in both sets of data. The sum of the capture kernels is slightly higher than the single value given in Refs. 23 or 24.

In the most recent documentation on nickel neutron-induced reaction cross-section evaluation for ENDF/B-V,[1] it is reported that "From 1.0×10^{-5} eV to 690.0 keV, the resonance parameters along with the smooth background cross sections have been taken from the ENDF/B-IV Ni evaluation which, in turn, were adopted from ENDF/B-III Ni evaluation." The ENDF/B-III ^{60}Ni resonance parameter evaluation was based on an evaluation by Stieglitz *et al.*[25] Forty-one s-wave resonances are reported from 12 to 652 keV but only 49 $l>0$ resonances from 1 to 553 keV. The radiation widths given in ENDF/B-V are average values based, for s-wave resonances, on the four values of Γ_γ obtained for resonances between 12 and 65 keV given in Table VI (Ref. 24). For $l>0$ (or p-wave) resonances $\bar{\Gamma}_\gamma$ is based on an unspecified number of radiation widths of resonances below 140 keV. The average radiation width of 2.14 eV given for s-wave resonances is large compared to our value of 1.30 ± 0.07 eV. The reason for this discrepancy is shown in the first two examples in Table VII which were discussed earlier. On the other hand, the average value of 0.6 eV given for the radiation width of the $l>0$ resonances is only half of our average Γ_γ of 1.2 eV which was calculated with all the non—s-wave resonances seen in both data sets and reported in Table II.

This new set of resonance parameters between 1 and 450 keV with the set of outside resonances necessary to describe the smooth background cross section is a definite improvement over the resonance parameters given presently in ENDF/B-V.

IX. DISCUSSION AND AVERAGE PARAMETERS

A. Reduced neutron width distribution of s-wave resonances

Thirty s wave resonances were identified in the range of energies analyzed, but some s-wave resonances of small width could have been missed. On the assumption that the reduced neutron widths of s waves follow a Porter-Thomas distribution,[26] an estimate of missed s wave resonances was made.

The reduced neutron width at 1 eV for s-wave resonances is

$$\Gamma_n^0=\Gamma_n\sqrt{1\text{ eV}/E_n}\ , \tag{9.1}$$

where E_n is in eV.

The normalized Porter-Thomas density function is

$$P(x)=(2\pi x)^{-1/2}e^{-x/2}\ , \tag{9.2}$$

where $x=\Gamma_n^0/\bar{\Gamma}_n^0$ and $\bar{\Gamma}_n^0$ is the average reduced neutron width.

The average of the 30 identified s-wave resonances reduced neutron widths is equal to 3.6 ± 0.4 eV. Since only resonances of small widths could have been missed, the value of $\bar{\Gamma}_n^0$ is possibly too large and the number of missed levels could be underestimated. The histogram giving the normalized reduced neutron widths, $\Gamma_n^0/\bar{\Gamma}_n^0$ for 29 of the 30 resonances identified as s waves in the analyzed region is given in Fig. 13. ($\Gamma_n^0/\bar{\Gamma}_n^0$ of the first s-wave resonance at 12.487 keV is equal to 5.9 and is not shown.) The smooth curve in Fig. 13 is the Porter-Thomas density function normalized to give the same number of levels under the curve as the observed number of levels in the range of values of x from 0.1 to 3.6. The normalization factor for the Porter-Thomas density function is 7.1 and is, as it should be, insensitive to the cutoff value of x used, since, when it is raised by a factor of 4 to 0.4, this normalization factor is 7.2. Comparing the number of levels observed with x values below 0.1 or below 0.4 with the corresponding area under the normalized Porter-Thomas density function yields the estimate that between three and four s-wave resonances having small neutron widths could have been missed.

B. Level densities

It is of some interest to determine within the framework of a model of level densities the con-

TABLE VII. Comparison of parameters obtained in this work for some overlapping resonances with parameters reported in earlier publications.

E_n[a] (keV)		$g\Gamma_n$	$g\Gamma_n\Gamma_\gamma/\Gamma$	Γ_γ	
$s_{1/2}$	$p_{1/2}$	(eV)	(eV)	(eV)	Reference
	42.705(1)	1.6(2)[c]	0.35(5)	0.45(3)	This work.
	42.985(2)[b]	2	0.37(4)	0.50[d]	See Fig. 8
43.105(1)		104.4(6)	0.26(2)	0.20(4)	
			0.98(7)		
43.050(4)		84.1(1)			22
42.92(11)				0.98(16)	23
43.08(23)		77(15)		1.73(18)	24
	64.918(10)[b]	0.05	0.05(2)[c]	0.50[d]	
	65.053(6)[b]	0.47	0.24(7)	0.50[d]	This work
65.228(1)		443.0(8)	1.10(5)	0.94(9)	
	65.573(2)[b]	≤ 2.4	1.09(8)	2.0	
			2.4(1)		
65.11(2)		459.9(8)			22
65.12(16)			1.9(3)		23
65.13(40)		390(30)		2.43(25)	24
	135.46(2)[b]	0.16	0.12(2)	0.50[d]	This work
	136.03(1)	15.5(4)	1.34(5)	1.45(8)	See Fig. 9
	136.29(1)	6.7(3)	1.93(8)	2.7(1)	
			3.4(1)		
	135.7(5)		3.3(5)		23
	136.5(14)		4.3(9)		24
139.03(1)		30.7(5)	1.14(6)	1.18(6)	This work.
	139.56(2)	26.2(5)	1.22(6)	1.28(7)	See Fig. 9
	140.01(1)	31.6(5)	2.23(6)	2.4(1)	
			4.6(1)		
	141.9	41.5(2.6)			22
	139.0(6)		3.0(5)		23
	139.6(14)		4.0(9)		24

[a]Resonance energy after all corrections discussed in Sec. VI were applied. Within parentheses are statistical uncertainties. The notation is such that $-0.15(11)$ stands for -0.15 ± 0.11. Same notation is used elsewhere in the table. See Sec. III for explanation of spin assignments.
[b]Resonance seen in capture only. If an upper bound of $g\Gamma_n$ is given, it is clearly seen as such on the theoretical fit to the transmission data and must be kept associated with the corresponding value of Γ_γ.
[c]Parameter adjusted by trial and error. The uncertainty was estimated from the sensitivity of the fit to the variation of this parameter.
[d]Assigned value of Γ_γ (see Sec. III for details).

sistency between the number of levels of different angular momentum observed in these experiments at high excitation energies in ^{61}Ni and the number of low-lying levels. The model used is the one of Gilbert and Cameron[27] where the Fermi-gas constant a and the energy shift parameter Δ are treated as free parameters.

Gilbert and Cameron started from a Fermi-gas model of the nucleus which was modified to take into account the pairing energy and possibly shell model effects, using an effective excitation energy U instead of the actual excitation energy E. The density of levels of total angular momentum J at an effective excitation energy U is given by

TABLE VIII. ^{60}Ni $l>0$ resonance capture kernels below 40 keV.

Present work		Fröhner, Ref. 23		Stieglitz *et al.*, Ref. 24	
E_n (keV)	$g\Gamma_n\Gamma_\gamma/\Gamma$ (eV)	E_n (keV)	$g\Gamma_n\Gamma_\gamma/\Gamma$ (eV)	E_n (keV)	$g\Gamma_n\Gamma_\gamma/\Gamma$ (eV)
2.253(1)	0.051[a]			2.257(9)	0.068(11)
5.532(1)	0.043(3)			5.53(2)	0.056(9)
12.220(1)	0.201(4)	12.23(3)	0.22(5)	12.2(4)	0.042(7)
13.624(1)	0.353(6)	13.62(3)	0.34(5)	13.6(5)	0.090(13)
		17.20(5)	0.06(2)		
21.274(2)	0.022(2)				
23.788(1)	0.24(1)	23.89(6)	0.72(12)	23.8(1)	0.92(14)
23.898(1)	0.54(1)				
28.458(2)	0.04(2)	28.47(7)	0.10(3)		
28.497(2)	0.11(2)				
29.480(2)	0.061(5)	29.46(8)	0.04(1)		
30.262(1)	0.39(1)	30.25(8)	0.34(5)	30.1(1)	0.32(5)
33.017(2)	0.56(1)	33.04(8)	0.40(7)	32.9(1)	0.35(6)
33.393(2)	0.29(1)	33.42(8)	0.23(4)	33.3(1)	0.19(3)
39.534(1)	0.57(1)	39.52(10)	0.43(7)	39.4(2)	0.57(10)

[a]Calculated with the parameters obtained from the transmission data analysis.

$$\rho(U,J)=\frac{\exp[2\sqrt{aU}\,]}{12a^{1/4}U^{5/4}}\,\frac{(2J+1)}{2\sqrt{2}}\times\frac{\exp[-(J+1/2)^2/2\sigma^2]}{\sigma^3}\,, \tag{9.3}$$

where a is the Fermi-gas constant and σ^2 is called the spin cutoff parameter. The effective excitation energy U is related to the actual excitation energy E above the ground state by the relation $U=E-\Delta$.

The spin cutoff parameter σ^2 is not a free parameter in the Fermi gas model since it is related to the distribution of the projections of the total angular momentum J. More specifically, the spin cutoff parameter is given by

$$\sigma^2=\frac{6}{\pi^2}\langle m^2\rangle\sqrt{aU}\,, \tag{9.4}$$

where $\langle m^2\rangle$ is the mean-square magnetic quantum number for single-particle states. From the shell model it is expected that

$$\langle m^2\rangle\simeq 0.146A^{2/3}\,, \tag{9.5}$$

where A is the atomic mass number of the compound system. This value of $\langle m^2\rangle$ will fluctuate somewhat due to shell effects. Combining those results we obtain

$$\sigma^2\simeq 0.0888A^{2/3}\sqrt{aU}\,. \tag{9.6}$$

This value of σ^2 corresponds approximately to the compound system having a moment of inertia equal to 75% of its rigid moment of inertia.[28]

If one adopts the above expression for σ^2, the Gilbert and Cameron level-density formula contains only two parameters: The Fermi-gas constant a and the energy shift factor Δ. The derivation of the above level density formula contains a number of approximations, and it is customary to treat the parameters a and Δ as free parameters which are adjusted to fit the data. It is within this framework

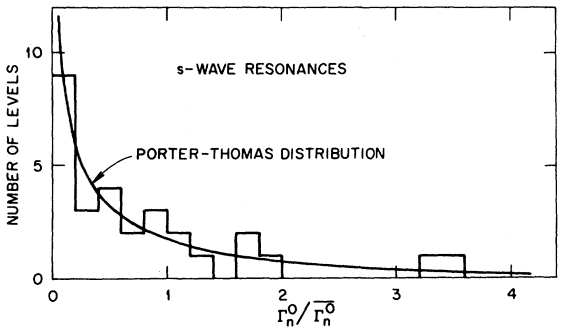

FIG. 13. The neutron reduced width distribution for the observed s-wave resonances. The smooth curve is the Porter-Thomas distribution normalized to the area of the histogram between $\Gamma_n^0/\overline{\Gamma}_n^0=0.1$ and 3.6.

that the level density formula above is being used.

Because of barrier penetrability effects we cannot use the number of $l>0$ resonances observed in this experiment in the fitting process to determine if there are values of a and Δ that are consistent with all the data since one does not know which J values they correspond to. However, one can use the number of s-wave resonances observed in the experiment together with the known[29] low-lying levels of ^{61}Ni. Then, using these values of a and Δ in the level density formula, one can compare its prediction for various l values with the observations made in this experiment for levels with $l>0$.

In the range of neutron energy from 10 to 450 keV, 30 s-wave resonances were observed, but, due to the possibly missed levels discussed in the previous section, this number of resonances is considered uncertain by three to four levels. We cannot expect that the level-density formula will reproduce correctly the density of very low-lying levels in ^{61}Ni due to the energy gap and collective effects which were not incorporated into the formula. Since the energy gap in ^{60}Ni extends to at least 2.1 MeV of excitation, we did not consider the levels below 2.1 MeV in ^{61}Ni as data that should be reproduced by the level-density formula. Also as the excitation energy in ^{61}Ni increases it is more likely that levels have been missed. On the basis of the data in the Nuclear Data Sheets,[29] it was decided that the level density formula should only be constrained to match the 13 levels observed in the range of 2.4 to 2.9 MeV with an uncertainty of ± 2 levels.

The values of the Fermi-gas constant a and the energy shift parameter Δ were obtained using the computer code LEVDEN.[30] LEVDEN is a fitting code that solves Bayes' equation. Using as prior values 6 ± 20 MeV^{-1} for the Fermi gas constant and 0 ± 2 MeV for the energy shift parameter, the code was required to produce 13 ± 2 levels of all values of J in the excitation energy interval 2.4 to 2.9 MeV above the ground state of ^{61}Ni and 30 ± 3 s-wave levels in the energy interval 10 to 450 keV above the neutron binding energy of 7.817 MeV in ^{61}Ni. This corresponds to a mean observed level spacing for s-wave resonances, D_0, equal to 15.2 ± 1.5 keV. The posterior values for the Fermi-gas constant and the energy shift parameter, with their standard deviations, were found to be

$$a=5.88\pm 0.24 \text{ MeV}^{-1}, \qquad \Delta=-0.77\pm 0.34 \text{ MeV} \tag{9.7}$$

with a correlation coefficient of 0.93.

The integral of the theoretical level density formula from 10 to 450 keV for $l=0$ with the above parameter values and their uncertainties is shown compared to the observed cumulative sum for s-wave resonances in Fig. 14 (bottom curve and staircase plot). Using the above parameter values and assuming that due to centrifugal barrier penetrabilities only $l=1$ and $l=2$ resonances were observed, the predictions of the model are compared to the cumulative sum of observed levels with $l>0$ also in Fig. 14. More $l>0$ levels have been observed than were predicted by the model using the above parameter values. We should not conclude that this disagreement indicates that we must be observing many resonances for which $l>2$ because it is possible to fit simultaneously the s-wave cumulative sum and the cumulative sum for $l>0$ resonances assuming that they contain only $l=1$ and $l=2$ levels at the expense of the fit to the number of low-lying levels in ^{61}Ni. For instance, the set of parameter values $a=6.5$ MeV^{-1} and $\Delta=0$ MeV in the level-density formula gives a very good fit to the observed cumulative sum of $l>0$ levels and gives 34 s-wave resonances from 10 to 450 keV, which is consistent with the observations if one includes the estimated missing levels. But it gives only nine levels in the energy range 2.4 to 2.9 MeV above the ground state of ^{61}Ni instead of 13. It is not clear to which extent one should reproduce the low-lying levels in ^{61}Ni due to collective effects that are ignored in the level density formula

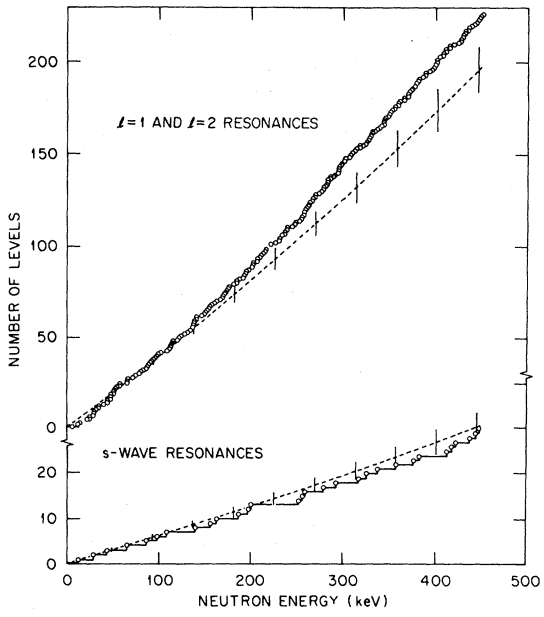

FIG. 14. Cumulative number of resonances for $l=0$ and $l=1$ and 2 as a function of the neutron incident energy. The dashed lines are fits to the data using the Fermi-gas model as discussed in Sec. IX B.

used. Another set of parameter values that reproduces well the cumulative sum of $l>0$ levels, assuming that they are only $l=1$ and $l=2$ levels, is $a=6.8$ MeV^{-1} and $\Delta=0.5$ MeV. This set of parameters also gives 34 s-wave resonances in the energy range from 10 to 450 keV but reduces to seven the number of levels in the 2.4 to 2.9 MeV energy range above the ground state of ^{61}Ni.

In view of the above, there seems to be little that one can conclude on the basis of the data obtained in these experiments concerning the validity of the Gilbert and Cameron level-density formulas treated as an empirical model.

C. s-wave strength function and doorway states

When discussing strength functions, it is useful to look at a plot of the cumulative sum of the reduced neutron widths of the observed resonances as a function of energy since the strength function defined as

$$S_0=\frac{\bar{\Gamma}_n^0}{D_0} \tag{9.8}$$

is the slope of such a plot. A plot of the cumulative sum of the s-wave resonances as a function of energy is shown in Fig. 15.

There is no ambiguity in obtaining the s-wave strength function from a staircase plot such as the one in Fig. 15 when it can be reasonably well approximated by a straight line over the complete energy range analyzed. When this is the case, the cumulative strength of the resonances being a linear function of the energy, the strength function is a very well defined entity and is independent of any method used for averaging. However, in many instances, as is the case for ^{60}Ni, the staircase plot shows considerable structure and it is necessary to consider the averaging procedure in some detail.

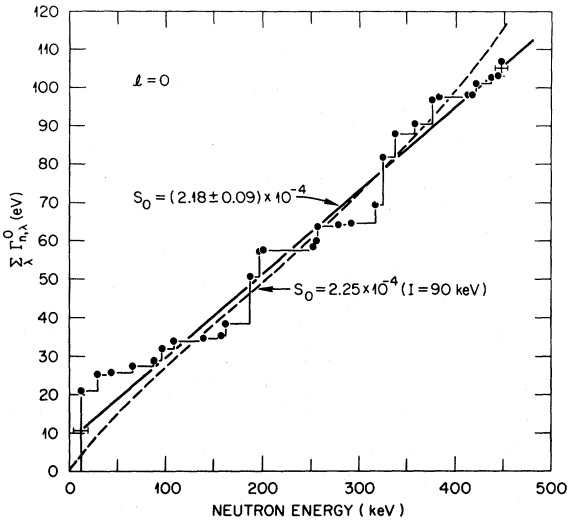

FIG. 15. The sum of the reduced neutron widths for s-wave resonances as a function of the neutron incident energy. The strength function is given by the slope of the full straight line or by the slope of the straight portion of the dashed line obtained by integrating, from 0 to 450 keV, the Lorentz-averaged strength function, S_{TOT}, with $I=90$ keV.

In Sec. IX A the distribution of the s-wave resonance reduced widths was analyzed within the framework of the Porter-Thomas distribution. It was found that for the 30 s-wave resonances observed up to 450 keV, the reduced widths were consistent with such a distribution. In Sec. IX B the level density from 0 to 450 keV was found to be consistent with a Fermi-gas model. The above indicate that the data are not inconsistent with the statistical assumptions that underlie these models. Assuming the validity of these statistical assumptions, the structure of the staircase plot in Fig. 15 is to be interpreted in terms of statistical fluctuations. A likelihood estimate could be made for the distribution of strength among pairs of nearest levels that are observed, for instance, by using a runs test. Although such a test was not made since the structure is clearly evident to the naked eye, it seems quite likely that a small probability would be found for the actual distribution observed. However, because the widths of these structures are rather small, the probability for the occurrence of these structures would not be so small as to compel us to reject the hypothesis of the statistical assumption with a null test.

In view of the above, the usual procedure for extracting the s-wave strength function could be followed. One notes that

$$\bar{\Gamma}_n^0=\frac{1}{N}\sum_{\lambda=1}^{N}\Gamma_{n,\lambda}^0 \tag{9.9}$$

and

$$D_0=(E_N-E_1)/(N-1)\,, \tag{9.10}$$

where E_1 is the energy of the first resonance analyzed and E_N the energy of the last one. From these observations, one obtains

$$S_0=\frac{N-1}{N}\frac{\sum_{\lambda=1}^{N}\Gamma_{n,\lambda}^0}{E_N-E_1}\,. \tag{9.11}$$

If one considers the uncertainties in the quantities that appear on the right-hand side of the expression, there is a very small uncertainty in the value of S_0 from the analysis of the data. However, as is well known,[31] if N levels are drawn randomly from a Porter-Thomas distribution having mean value $\overline{\Gamma}^0_n$, the expectation value in the sum of these N levels is $N\overline{\Gamma}^0_n$ and the variance in this sum is $2N(\overline{\Gamma}^0_n)^2$. Therefore, even though we may have obtained with great accuracy the total strength in the energy interval 0 to 450 keV, there is a relative standard deviation of $\sqrt{2/N}$ or 26% in the numerator of S_0. In comparison the uncertainty in $E_N - E_1$ is small even though one could argue that since the full strength of the first and last resonances is taken in the summation of the reduced neutron widths, half of the average level spacing D_0 should be added at each end of the energy interval $E_N - E_1$. The maximum uncertainty on the denominator would still be only 3%. The strength function calculated with relation (9.11) is equal to $(2.38 \pm 0.62) \times 10^{-4}$.

Relation (9.11) can be considered as determining the average value of the strength function at the energy which is the midpoint of the energy range analyzed, and a rectangular weighting function is used whose width is equal to the energy range analyzed. As is well known, such sharp weighting functions have very unpleasant mathematical properties. This can be illustrated in our case by eliminating the lowest and highest energy resonances analyzed. One now obtains a nominal value for S_0 of 1.9×10^{-4}. It can be observed from Fig. 15 that subsequent reductions in the width of the rectangular weighting function will produce much smaller changes. A compromise value is suggested for the nominal value of the "statistical" strength function. It is given by the slope of the "best line" fit that goes through two rectangular boxes centered at the energies of the lowest and highest resonance analyzed as shown in Fig. 15. The widths of these boxes are equal to the average level spacing and the heights to the reduced widths of these resonances. The value so found is 2.18×10^{-4} with a standard deviation of 0.09×10^{-4}. This line appears suggestively to be a good straight-line approximation to the staircase plot over the complete energy range. This value of 2.18×10^{-4} represents a minimal attempt at mitigating the sharpness of the weighting function.

The s-wave neutron strength function recommended in Ref. 32 for ^{60}Ni in the 0 to 600 keV energy range is $(2.7 \pm 0.6) \times 10^{-4}$. Fröhner[23] reports a value of $(2.6 \pm 0.8) \times 10^{-4}$ and Stieglitz *et al.*[24] a value of $(2.95 \pm 1.04) \times 10^{-4}$ from their analyses up to 340 keV.

There are three conspicuous large steps in the staircase plot in Fig. 15 occurring at 15, 190, and 325 keV. They arise because two consecutive levels have relatively large reduced widths in the first two steps and three in the third step. These steps account for 63% of the total s-wave strength in the energy region analyzed but span only about 10% of the energy range. Although as pointed out, it is not unlikely that these steps arise from purely statistical sources, they could be the manifestation of some nuclear physical mechanism modulating the strength of the levels in this energy region. They could indicate the presence of particle-vibration doorway states and, if this were so, one should find such modulations of the s-wave strength function in the nuclides of this mass region. Such modulations have been observed before. In ^{54}Fe where the level spacing is also large[23]—of the order of 20 keV—two large steps occur in the cumulative s-wave strength as a function of energy. They are located around 192 and 330 keV. In the zinc isotopes, ^{66,68,70}Zn, where level spacing is of the order of 5 keV, these modulations also occur but are spread over many more levels.[34] Preliminary calculations[35] indicate that these modulations could be due to particle-vibration doorway states.

If one is interested in studying modulations of the strength function in terms of doorway states, it is convenient to average the reduced R function with a Lorentzian weighting function.[36] The poles of the Teichman-Wigner reduced R function[37] are necessarily below the energy axis, and we have

$$R(E) = \sum_\lambda \frac{\gamma_{n,\lambda}{}^2}{E_\lambda - E - i\gamma_{e,\lambda}{}^2/2}, \tag{9.12}$$

where in our case $\gamma_{e,\lambda}{}^2$'s are the effective reduced level widths for the eliminated channels: the capture channels. It should be noted that the sum is to be carried over all the poles of the R function, that is to say, should include the poles outside the energy region analyzed. Because the poles of the reduced R function are below the real axis, if one calculates the R function at an energy $E + iI$, where I is a positive number, one is calculating an average value of the R function at the energy E. The amount of averaging that one performs is controlled by the size of I. In the statistical model, one makes I very large compared to the averaged level spacing in order to completely average over the statistical fluctuations. If the level widths have a Porter-Thomas distribution, I must also be very large in order to effectively average over the fluctuations. The value of the R function at a complex energy $E + iI$ where $I \gg \gamma_{e,\lambda}{}^2$ is usually denoted by

$$R(E+iI)=\bar{R}(E,I)+i\pi S(E,I)\ , \tag{9.13}$$

where

$$\bar{R}(E,I)=\sum_{\lambda}\frac{\gamma_{n,\lambda}^{2}(E_{\lambda}-E)}{(E_{\lambda}-E)^{2}+I^{2}} \tag{9.14}$$

and

$$S(E,I)=\frac{I}{\pi}\sum_{\lambda}\frac{\gamma_{n,\lambda}^{2}}{(E_{\lambda}-E)^{2}+I^{2}}\ . \tag{9.15}$$

Because of the factor $E_{\lambda}-E$ in the numerator, $\bar{R}(E,I)$ is often called the contribution of the distant levels, away from the value of E, to the average. The absence of such a factor in the numerator of $S(E,I)$ means that its value at the energy E is more strongly dominated by the levels near the energy E and $S(E,I)$ is often called the Lorentzian averaged strength function.

We show in Fig. 16 the value of $S(E,I)$ for several values of I, from twice the average level spacing D_0 to six times D_0 over the range of energy the data were analyzed. The cumulative sum of the reduced level widths and the reduced level widths for the levels in the region analyzed are also shown for comparison. In Fig. 17, the contributions of the levels inside the energy region analyzed, $S_{\rm int}$, and those of the levels outside of the energy region, $S_{\rm ext}$, are shown. It should be noted that the levels outside the energy region analyzed are not "physical levels" in the sense that we expect actual resonances or states to be observed there. These external levels are merely an expansion of the contribution of the levels outside the energy region to the R function inside the energy range analyzed. These contributions must be included in any analysis in order to fit the data but are often not represented by a pole expansion except for a single negative energy resonance.

The integral from 0 to 450 keV of the total Lorentz-weighted strength function averaged with $I=90$ keV (six times the averaged level spacing) is given by the dashed line in Fig. 15. The slope of the straight part of this line gives also an estimate of S_0 in the middle of the range of energy analyzed and is found to be equal to 2.25×10^{-4}.

In Fig. 18, the value of $\bar{R}(E,I)$ corresponding to the value of $S(E,I)$ in Fig. 17 is shown. However, because $\bar{R}(E,I)$ is more sensitive to far away levels, due to the term $(E_{\lambda}-E)$ in the numerator, there is very little that one can infer about its behavior. The pole expansion used for the contribution of the levels outside the energy region analyzed is largely in-

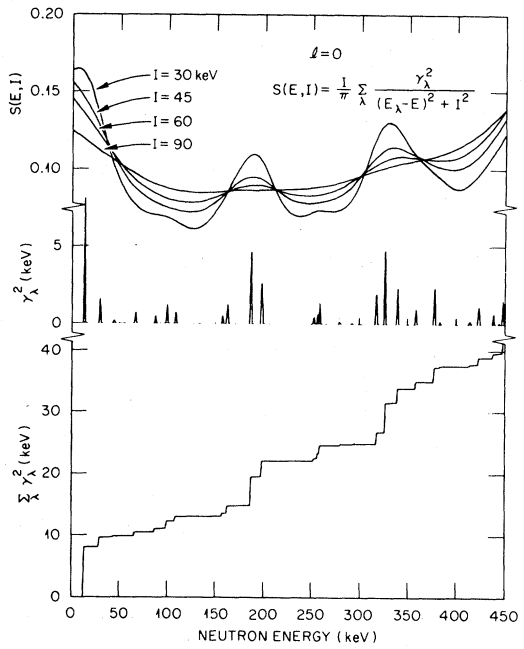

FIG. 16. From top to bottom: the Lorentz-weighted strength function of the reduced level widths of the observed s-wave resonances averaged over various energy intervals; the reduced level widths of the observed s-wave resonances; summations of the reduced level widths of the s-wave resonances as a function of the neutron incident energy. The three doorway states are clearly seen on each of these representations of the s-wave resonances reduced level widths.

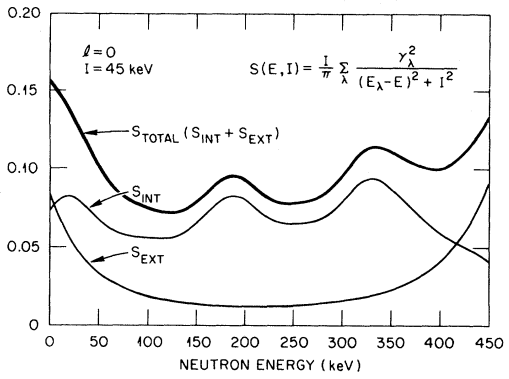

FIG. 17. Lorentz-weighted s-wave strength function of the reduced level widths averaged with $I=45$ keV between 0 and 450 keV. $S_{\rm INT}$ is the contribution of the 30 observed s-wave resonances inside the 0- to 450-keV region. $S_{\rm EXT}$ is the contribution of the ten outside resonances. $S_{\rm TOTAL}$ is the sum of $S_{\rm INT}$ and $S_{\rm EXT}$.

sensitive to the faraway levels.

Figure 16 displays very graphically the modulation of strength of the levels in the energy region analyzed and is suggestive of possible doorway states at least around 190 and 325 keV. There is very little that can be done with our data to investigate the possibility that there may be additional structure below the energy range analyzed. However, this can be done above 450 keV. In our preliminary analysis using the code MULTI, the analysis of the transmission data had been carried out to 550 keV. As is evident from the capture data above 450 keV, there is a high density of levels in the 450—550 keV region, and it is judged that a large part of subjectivity entered in the analysis, in particular concerning the smaller levels. However, one can be fairly confident in the analysis concerning the large s-wave resonances. Plots similar to the ones shown in Figs. 15 and 17 were made for $l=0$ resonances up to 550 keV and are given in Ref. 2. Indeed, another possible doorway state is evident around 510 keV.

We conclude that even though the distribution of reduced level widths follows the Porter-Thomas distribution, there may be particle-vibration doorway states responsible for the modulation as a function of energy of the strengths of the s-wave levels. This will be investigated theoretically and an attempt made to see if such particle-vibration doorway states can provide a coherent explanation of the behavior of the reduced level width distributions as a function of energy observed for nuclides in this mass region.

D. Correlation between Γ_n^0 and Γ_γ for s-wave resonances

Because a correlation between the reduced neutron widths and the radiation widths of the observed resonances might indicate nonstatistical effects, such correlation coefficients are frequently calculated for s-wave resonances. The relationship between the Γ_n^0 and Γ_γ correlation coefficients and the results given by the valence model calculations were discussed by Allen *et al.*[38] in the case of ^{54}Fe.

A survey of correlation coefficients for nuclei in the mass region $40<A\leq 64$ was made by Beer and Spencer[39] in 1975. Only a few resonances were available for each isotope. For ^{60}Ni the reported correlation coefficient of 0.8 ± 0.28 was based on nine s-wave resonances below 170 keV, and it was shown that this correlation was due entirely to the single large resonance at 12.5 keV.

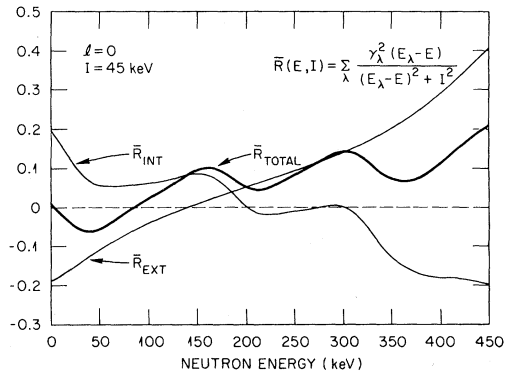

FIG. 18. Lorentz-weighted R function of the s-wave reduced level widths averaged with $I=45$ keV between 0 and 450 keV. $\bar{R}_{INT}$ is the contribution of the observed 30 s-wave resonances inside the 0- to 450-keV region. $\bar{R}_{EXT}$ is the contribution of the ten outside resonances. $\bar{R}_{TOTAL}$ is the sum of $\bar{R}_{INT}$ and $\bar{R}_{EXT}$.

TABLE IX. Correlation coefficients $\rho(\Gamma_n^0,\Gamma_\gamma)$ for some medium-weight nuclei.

Element	J	No. of s-wave resonances	$\rho(\Gamma_n^0,\Gamma_\gamma)$	Reference
^{55}Mn	2,3	47	0.64±0.14	40
^{54}Fe	$\frac{1}{2}$	16	0.94±0.49	41
^{56}Fe	$\frac{1}{2}$	15	0.34±0.20	41
^{59}Co	3,4	35	0.33±0.06	42
^{60}Ni	$\frac{1}{2}$	30	0.53±0.18	This work
^{64}Zn	$\frac{1}{2}$	32	0.47±0.08	43
^{66}Zn	$\frac{1}{2}$	26	0.59±0.10	34
^{68}Zn	$\frac{1}{2}$	22	0.5	34

Since then analyses of high-resolution ORELA data for medium-weight nuclei were completed and correlation coefficients were calculated for a large number of resonances. These correlation coefficients are given in Table IX for eight nuclei in the mass region $54 \leq A \leq 68$ for a total of 223 resonances. The correlation coefficients given for the iron isotopes were calculated from the recommended parameter values of Ref. 41. The uncertainties quoted include uncertainties in the neutron and radiation widths and the effect of finite sample size. The results of Allen and Macklin[44] for ^{58}Fe are not given in this paper because of difficulties in identifying which of the resonances are s waves and because of problems with other isotopes in the samples.[45]

The correlation coefficient for the 30 s-wave resonances of ^{60}Ni analyzed in this work is 0.53 ± 0.18. As expected the parameters of the large resonance at 12.487 keV are no longer dominant. Without the parameters of this resonance the correlation coefficient is 0.48 ± 0.15.

The 50% uncertainty on the neutron sensitivity correction factor is the major source of uncertainty on the radiation widths of large s-wave resonances as discussed in Sec. V. In other publications[34,40,42,43] a smaller uncertainty on this correction factor was assumed which explains the smaller uncertainties on the correlation coefficients reported for ^{55}Mn, ^{59}Co, and zinc isotopes than we have for ^{60}Ni.

We investigated the sensitivity of the correlation coefficient to the absolute normalization of the neutron sensitivity curve used for the detector in the capture measurements (Fig. 12). If the neutron sensitivity coefficients C in Table II are lowered systematically by a factor of 2, the correlation coefficient would increase from 0.53 to 0.68 ± 0.17. If they are systematically increased by a factor of 1.5, then the correlation coefficient decreases to a value of 0.38 ± 0.18.

It seems that in this mass region the correlation coefficients are of the order of 0.5. This result could be considered evidence for nonstatistical effects in these nuclei as well as the structure observed in the reduced width staircase plots.

E. Average capture cross sections

The average capture cross sections given in the first two sections of Table X in lethargy intervals up to 450 keV were obtained by summing the capture areas of the resonances in each interval. The "narrow resonance" approximation was made; that is to say, the entire capture area of the resonance was assumed to fall in the energy interval where the resonance energy lies. This approximation is very poor only for the large s-wave resonance at 12.487 keV. The uncertainties include the statistical uncertainties as well as the uncertainties from the correction for the detector neutron sensitivity. The uncertainties in

TABLE X. Average capture cross sections. Up to 450 keV, the average capture cross sections were calculated from the resonance parameters obtained in this analysis. Uncertainties due to the prompt neutron sensitivity of the detector combined with the statistical uncertainties are given. From 400 keV, and up to the inelastic threshold, $\bar{\sigma}_\gamma$ was estimated directly from the thick sample capture data. Statistical uncertainties are given. Corrections applied to the data in this energy range and systematic uncertainties are discussed in Sec. IX E.

Energy range (keV)	Average capture cross sections (mb)	Energy range (keV)	Average capture cross sections (mb)	Energy range (keV)	Average capture cross sections (mb)
2.0–2.51	188 ± 4				
5.0–6.3	25.3± 0.6	50.1±63.1	9.8±0.1	400–500	8.5±0.1
6.3–7.9		63.1–79.4	13.7±0.5	500–600	7.8±0.1
7.9–10.		79.4–100.	19.4±0.8	600–700	8.0±0.1
10–12.6	366 ±114	100–126	12.8±0.3	700–800	7.4±0.1
12.6–15.8	34.3± 0.6	126–158	13.6±0.2	800–900	8.4±0.1
15.8–20		158–200	14.2±0.4	900–1000	7.8±0.1
20.–25.1	28.0± 0.5	200–251	9.3±0.2	1000–1100	8.0±0.2
25.1–31.6	29± 11	251–316	10.0±0.2	1100–1200	9.6±0.2
31.6–39.8	20.7± 0.4	316–398	11.8±0.3	1200–1300	10.6±0.2
39.8–50.1	19.4± 0.9	398–450	9.6±0.2		

the correction for the detector neutron sensitivity were treated as uncorrelated, a poor approximation when the correction curve is smooth. To these uncertainties, the systematic uncertainties discussed in Sec. VII B *3* should be added and treated as fully correlated. The average capture cross section given in the 2.0 to 2.5 keV interval was calculated from the resonance parameters obtained in the transmission data analysis of the 2.253-keV resonance.

From 400 keV to the threshold of the inelastic scattering to the first 2^+ state in ^{60}Ni (1355 keV), the thick sample data were corrected for average resonance self-protection and scattering of neutrons in the sample before capture using strength functions. While this is admittedly a poor substitute for individual resonance parametrization as was done below 450 keV, the corrections to the data were small, 2.4% at 450 keV dropping to 0.4% at 1250 keV. The 2.5-mb background found between resonances at lower energies, discussed in Sec. V, was subtracted. The uncertainty in this background correction is the dominant uncertainty and should be considered fully correlated. The average capture cross sections above 400 keV are given in the third section of Table X and the uncertainties are the statistical uncertainties only.

The average cross sections up to 1 MeV are shown in Fig. 19, together with a theoretical calculation. The theoretical calculation was provided by C. Y. Fu and obtained using the code TNG.[46] The code TNG calculates the capture cross sections by using transmission coefficients for gamma rays derived from the width of the $E1$ giant dipole resonance.[47] Only $E1$ transitions were considered and the gamma ray partial widths are only functions of the gamma-ray energy E_γ, the initial level spin, and the final level spin. Level densities and their spin distributions were obtained from the Gilbert-Cameron formula. The parameters of the giant dipole resonance for ^{60}Ni were taken from the photonuclear reaction data[48] ($\sigma_0=90$ mb, $E_0=19.0$ MeV, and the Lorentzian width of 5.5 MeV). This model usually predicts the capture cross sections within a factor of 2.[47] In this case, the capture cross section was overpredicted and the theoretical predictions in Fig. 19 were normalized by a factor of 0.40.

For comparison with our results, the average capture cross section was calculated with the parameters given in ENDF/B-V. Since ENDF/B-V does not have an isotopic evaluation of ^{60}Ni, the resonance parameters were taken from the elemental evaluation of nickel. In ENDF, the capture cross section is calculated using the resonance parameters to which is added a smooth background. In the evaluation of elemental nickel, the smooth background is of the order of 6 mb. If we assume that

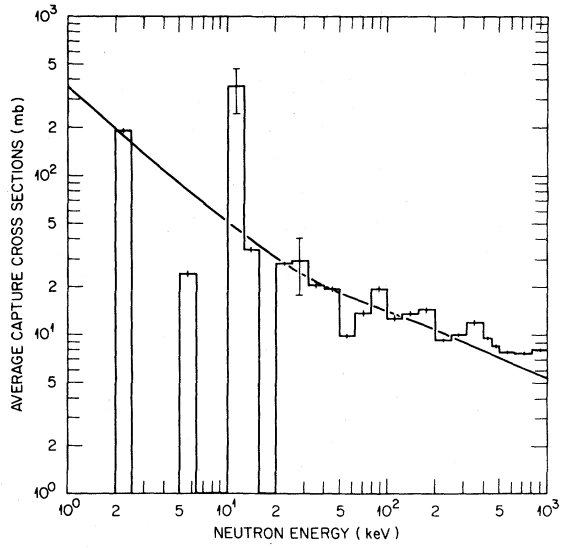

FIG. 19. ^{60}Ni average capture cross section from 2 keV to 1 MeV as a function of the neutron incident energy. The smooth curve is given by the tail of the giant dipole at 19 MeV normalized by a factor of 0.40.

this 6-mb background is to be added to all the isotopes of nickel, we can calculate the ENDF/B-V average capture cross section, which, when compared to our results indicates that the ENDF/B-V infinitely dilute capture cross section for ^{60}Ni above 20 keV is approximately 20–25 % smaller than our results shown in Fig. 19.

The first s-wave resonance at 12.487 keV contributes 1.5 ± 0.5 b to the thermal capture cross section. Summing the contributions of the other 29 s-wave resonances at positive energies up to 450 keV gives only an additional 0.03 b. The latest evaluation of the thermal capture cross section[32] gives 2.9 ± 0.2 b. The difference could be attributed to the direct capture component and to bound levels but the data analyzed in this report are not sensitive to these contributions.

X. CONCLUSION

The number of analyzed resonances for ^{60}Ni reported in this paper between 1 and 452 keV is more than three times the number of resonances previously identified in this energy region. A total of 255 resonances is given, of which 166 were seen in both sets of data and 89 were seen in the capture data only. The radius parameter of 6.0 fm and the ten

fictitious s-wave resonances must be kept associated to this set of resonance parameters to properly describe the transmission data below 452 keV. From the 30 observed s-wave resonances, the average level spacing was found to be equal to 15.2 ± 1.5 keV, the strength function to $(2.2\pm0.6)\times10^{-4}$ and the average radiation width to 1.30 ± 0.07 eV. Although the distribution of the s-wave resonance reduced neutron widths is in good agreement with a Porter-Thomas distribution, the strength of the s-wave resonances is modulated in a way that is suggestive of doorway states as observed in other nuclides in this mass region. The correlation coefficient of 0.53 ± 0.18 observed between the reduced neutron widths and the radiation widths of the s-wave resonances is also suggestive of nonstatistical effects.

ACKNOWLEDGMENTS

We gratefully acknowledge the valuable assistance of N. W. Hill in the experimental aspects of the transmission measurements and the extensive help of N. M. Larson during the analysis of the transmission data with the code SAMMY. We thank W. M. MacDonald and D. J. Horen for providing the codes used to perform the Lorentzian averaging of the R function. We also thank C. Y. Fu for performing the average capture cross-section prediction calculations and R. R. Spencer for helpful discussions on the correlation coefficient between the resonance widths. This research was sponsored by the Division of Basic Energy Sciences, U. S. Department of Energy, under Contract No. W-7405-eng-26, with the Union Carbide Corporation.

[1]M. Divadeenam, Brookhaven National Laboratory Report No. BNL-NCS-51346, 1979 (unpublished).

[2]C. M. Perey, J. A. Harvey, R. L. Macklin, R. R. Winters, and F. G. Perey, Oak Ridge National Laboratory Report No. ORNL-5893, 1982 (unpublished).

[3]N. W. Hill, J. A. Harvey, G. S. Slaughter, and A. St. James, Bull. Am. Phys. Soc. 17, 901 (1972). [Also in Oak Ridge National Laboratory Physics Division Annual Progress Report 1971, ORNL-4743 (unpublished), p. 137.]

[4]D. C. Larson, C. H. Johnson, J. A. Harvey, and N. W. Hill, Oak Ridge National Laboratory Report No. ORNL/TM-5612, 1976 (unpublished). Also see Ref. 17.

[5]M. S. Pandey, J. B. Garg, and J. A. Harvey, Phys. Rev. C 15, 600 (1977).

[6]N. A. Betz, J. W. Reynolds, and G. G. Slaughter, in the Proceedings of the Conference on Computer Systems in Experimental Nuclear Physics, Skytop, Pennsylvania, 1969, Columbia University Report No. CONF-690301 (unpublished), p. 218.

[7]G. F. Auchampaugh, Los Alamos National Laboratory Report No. LA-5473-MS, 1974 (unpublished).

[8]N. M. Larson and F. G. Perey, Oak Ridge National Laboratory Report No. ORNL/TM-7485, 1980 (unpublished).

[9]F. G. Perey, G. T. Chapman, W. E. Kinney, and C. M. Perey, in *Neutron Data of Structural Materials for Fast Reactors, Geel, 1977,* edited by K. H. Böckhoff (Pergamon, New York, 1979), p. 530.

[10]D. J. Horen, J. A. Harvey, and N. W. Hill, Phys. Rev. C 20, 478 (1979).

[11]R. L. Macklin and B. J. Allen Nucl. Instrum. Methods 91, 565 (1971).

[12]R. L. Macklin, N. W. Hill, and B. J. Allen, Nucl. Instrum. Methods 96, 509 (1971).

[13]R. L. Macklin, R. W. Ingle, and J. Halperin, Nucl. Sci. Eng. 71, 205 (1979).

[14]R. L. Macklin, J. Halperin, and R. R. Winters, Nucl. Instrum. Methods 164, 213 (1979).

[15]R. L. Macklin, Oak Ridge National Laboratory Report No. ORNL/TM-4810, 1975 (unpublished); see also Nucl. Sci. Eng. 59, 12 (1976), especially the Appendix.

[16]B. J. Allen, A. R. de L. Musgrove, R. L. Macklin, and R. R. Winters, in Ref. 9, p. 506.

[17]D. C. Larson, J. A. Harvey, N. W. Hill, and C. H. Johnson, Oak Ridge National Laboratory Report No. ORNL/TM-8203, 1982 (unpublished).

[18]F. G. Perey, Evaluated Nuclear Data File No. 300, 1979 (unpublished), p. IX. 1.

[19]J. Halperin, C. H. Johnson, R. R. Winters, and R. L. Macklin, Phys. Rev. C 21, 545 (1980).

[20]C. Coceva, R. Simonini, and D. K. Olsen, Nucl. Instrum Methods (to be published).

[21]H. Beer and R. L. Macklin, Phys. Rev. C 26, 1404 (1982).

[22]D. B. Syme, P. H. Bowen, and A. D. Gadd, in Ref. 9, p. 703.

[23]F. Fröhner, in Ref. 9, p. 138; F. Fröhner, in *Neutron Physics and Nuclear Data for Reactors, Harwell, 1978* (OECD, Paris, 1978), p. 268.

[24]R. G. Stieglitz, R. W. Hockenbury, and R. C. Block, Nucl. Phys. A163, 592 (1971).

[25]R. G. Stieglitz, J. T. Reynolds, C. J. Slavik, and C. R. Lubitz, Knolls Atomic Power Laboratory Report No. KAPL-M-7156, 1973 (unpublished).

[26]C. E. Porter and R. G. Thomas, Phys. Rev. 104, 483 (1956).

[27]A. Gilbert and A. G. W. Cameron, Can. J. Phys. 43, 1446 (1965).

[28]W. Dilg, W. Schantl, H. Vonach, and M. Uhl, Nucl. Phys. A217, 269 (1973).

[29]J. Vereier, Nucl. Data, B2 (No. 5), 1968, p. 99.
[30]N. M. Larson (private communication).
[31]J. E. Lynn, *The Theory of Neutron Resonance Reactions* (Clarendon, Oxford, 1968).
[32]S. F. Mughabghab, M. Divadeenam, and N. E. Holden, *Neutron Cross Sections, Vol. 1: Neutron Resonance Parameters and Thermal Cross Sections* (Academic, New York, 1981), p. 28-8.
[33]M. S. Pandey, J. B. Garg, J. A. Harvey, and W. M. Good, NBS Special Publication No. 425, 1975 (unpublished).
[34]J. B. Garg, V. K. Tikku, J. A. Harvey, R. L. Macklin, and J. Halperin, Phys. Rev. C 24, 1922 (1981); J. B. Garg, V. K. Tikku, J. A. Harvey, J. Halperin, and R. L. Macklin, *ibid.* 25, 1808 (1982); J. B. Garg, V. K. Tikku, and J. A. Harvey, Phys. Rev. C (to be published).
[35]J. A. Harvey, M. Divadeenam, J. B. Garg, and V. K. Tikku, Bull. Am. Phys. Soc. 26, 1138 (1981); J. B. Garg, V. K. Tikku, J. A. Harvey, R. L. Macklin, and M. Divadeenam, Bull. Am. Phys. Soc. 26, 1138 (1981).
[36]C. Mahaux and H. A. Weidenmuller, Nucl. Phys. A91, 241 (1967); W. M. MacDonald and A. Z. Mekjian, Phys. Rev. 160, 730 (1967); A. K. Kerman and A. F. R. de Toledo Piza, Ann. Phys. (N.Y.) 48, 173 (1968).
[37]T. Teichmann and E. P. Wigner, Phys. Rev. 87, 123 (1952).
[38]B. J. Allen, A. R. de L. Musgrove, J. W. Boldeman, and R. L. Macklin, Nucl. Phys. A283, 37 (1977).
[39]H. Beer and R. R. Spencer, Nucl. Phys. A240, 29 (1975).
[40]J. B. Garg, R. L. Macklin, and J. Halperin, Phys. Rev. C 18, 2079 (1978).
[41]C. M. Perey and F. G. Perey, Oak Ridge National Laboratory Report No. ORNL/TM-6405, 1980 (unpublished).
[42]R. R. Spencer and R. L. Macklin, Nucl. Sci. Eng. 61, 346 (1976).
[43]J. B. Garg, V. K. Tikku, J. Halperin, and R. L. Macklin, Phys. Rev. C 23, 683 (1981).
[44]B. J. Allen and R. L. Macklin, J. Phys. G 6, 381 (1980).
[45]F. Käppeler, K. Wisshak, L. D. Hong, Nucl. Sci. Eng. (to be published).
[46]C. Y. Fu, NBS Special Publication No. 425, 1975 (unpublished).
[47]P. Axel, Phys. Rev. 126, 671 (1962).
[48]E. G. Fuller, H. M. Gerstenberg, H. Vander Molen, and T. C. Dunn, NBS Special Publication No. 380, 1973 (unpublished).